Title

Propane Dehydrogenation and Cracking over Zn/H-MFI Prepared by Solid-State Ion Exchange of ZnCl2

Journal

ACS Catalysis, 11(23)

ISSN

2155-5435

Authors

Nozik, Danna
Tinga, Francesca Mikaela P
Bell, Alexis T

Publication Date

2021-12-03

DOI

10.1021/acscatal.1c03641

Peer reviewed

ACS Catalysis

pubs.acs.org/acscatalysis

Research Article

Propane Dehydrogenation and Cracking over Zn/H-MFI Prepared by Solid-State Ion Exchange of $ZnCl_2$

Danna Nozik, Francesca Mikaela P. Tinga, and Alexis T. Bell*

Cite This: *ACS Catal.* 2021, 11, 14489–14506

Read Online

ACCESS | Metrics & More | Article Recommendations | Supporting Information

ABSTRACT: Light alkanes in shale gas are an attractive source of carbon for the production of alkenes and aromatics compared to petroleum-derived naphtha. Zinc-exchanged zeolite H-MFI (Zn/H-MFI) is active and selective for light alkane dehydrogenation and dehydroaromatization. In this study, Zn/H-MFI with varying Zn/Al ratios was prepared via solid-state ion exchange (SSIE) of $ZnCl_2$ and characterized by various methods. As-prepared Zn/H-MFI with Zn/Al $\leq$ 0.52 contains isolated $[ZnCl]^+$ and $[ZnCl(HCl)]^+$ species; Zn/H-MFI with higher Zn loadings also contains $ZnAl_2O_4/ZnAl_2O_{4-x}Cl_{2x}$ nanoclusters. Postsynthetic treatment in He and subsequently in 2.5% H_2 in He at 773 K removes Cl and adsorbed HCl, resulting in the formation of $[ZnH]^+$ cations. Studies of C_3H_8 dehydrogenation and cracking suggest that in the absence of cofed H_2, $[ZnH]^+$ cations are transformed to bridging Zn^{2+} cations, which exhibit higher C_3H_8 dehydrogenation activity and selectivity relative to $[ZnH]^+$ cations. The kinetics of dehydrogenation and cracking over Zn/H-MFI were investigated as a function of Zn loading, C_3H_8 partial pressure, and temperature. The turnover frequency for propane dehydrogenation and cracking increases with Zn loading, which we propose is due to localization of Zn^{2+} cations either at increasingly distant pairs of Al atoms or at the β-site in the MFI framework. The selectivity to dehydrogenation over cracking over Zn^{2+} is independent of C_3H_8 partial pressure and temperature, consistent with dehydrogenation and cracking pathways that proceed via a common surface intermediate and have similar enthalpies of activation. The product distribution is thus determined by the entropy of activation for each pathway, which is less negative in the case of C_3H_8 dehydrogenation.

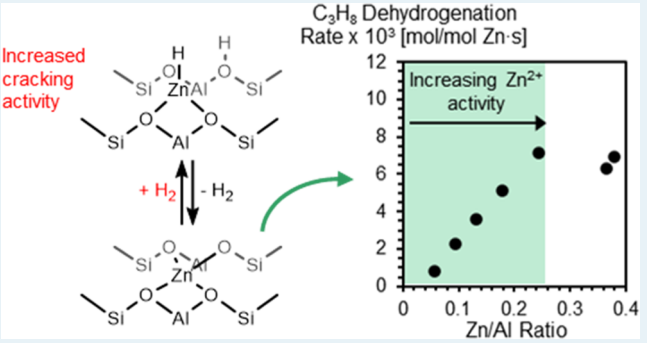

KEYWORDS: *Zn/H-MFI, zinc, zeolite, propane dehydrogenation, zinc chloride, solid-state ion exchange, catalyst characterization, kinetics*

1. INTRODUCTION

Increasing shale gas production in the United States has incentivized the conversion of light alkanes derived from shale gas to alkenes and aromatics, primarily benzene, toluene, and xylenes (BTX). BTX are traditionally produced via catalytic reforming of naphtha and are important feedstocks for the production of plastics, fibers, resins, and films.[1−4] Prior work has shown that dehydroaromatization involves initial alkane dehydrogenation to form alkenes, which then undergo oligomerization, cyclization, and further dehydrogenation to form the final aromatic products. Lewis acidic metal cations exchanged into zeolites are used industrially to catalyze the dehydrogenation and subsequent aromatization of light alkanes. In particular, BP/UOP's Cyclar process utilizes Ga/H-MFI zeolites for the dehydroaromatization of C_3-C_4 alkanes.[1−4] While Ga/H-MFI has been explored extensively for this purpose, the Ga hydride species contained in this catalyst ($[GaH]^{2+}$ and $[Ga(H)_2]^+$ cations) are active for alkane cracking as well as dehydrogenation.[5−7] For this reason, and because Ga is a relatively expensive element, efforts have been undertaken to find a more earth-abundant element and one that would exhibit low selectivity to alkane cracking.

A number of researchers have identified zinc-exchanged H-MFI zeolites (Zn/H-MFI) as active and selective catalysts for light alkane dehydrogenation. While the volatility of Zn has been noted as a drawback to the use of Zn/H-MFI,[8] it has been reported that Zn/H-MFI can be prepared such that Zn sublimation does not occur during propane dehydrogenation and dehydroaromatization.[9]

The method of Zn/H-MFI preparation is known to affect the nature of Zn species formed.[10−28] Various methods have been used to introduce Zn into MFI. These include aqueous ion exchange[10−16] and incipient wetness impregnation of dissolved $Zn(NO_3)_2$[10,13−15] and sublimation of $ZnCl_2$,[16−18]

Received: August 11, 2021
Revised: October 28, 2021
Published: November 17, 2021

Table 1. Effect of Preparation Method on the Structure of Zn Species in Zn/H-MFI and Zn/Na-MFI[a]

	structure of the Zn species formed						
preparation method	Zn^{2+} and/or $[ZnOH]^+$	Zn^{2+}-O-Zn^{2+}	$Zn_nO_m^{a+}$	ZnO	Zinc oxychlorides	$[ZnCl]^+$	Zn^0
aqueous ion exchange into H-MFI	10−16						
aqueous ion exchange into Na-MFI	12	12					
incipient wetness impregnation	10, 13−15		13	10, 13−15			
sublimation of $ZnCl_2$	16, 18			16	17	16, 18	
sublimation of ZnO	16			15, 16			
sublimation of dimethylzinc	13		13	13			
sublimation of Zn metal	13, 21−29		21−23				13

[a]Table elements indicate the references that have reported the formation of the particular Zn species in Zn/H-MFI or Zn/Na-MFI as a result of the particular preparation method.

ZnO,[15,16] dimethylzinc,[13] and Zn metal.[13,19−28] Table 1 summarizes species reported as a function of the method of Zn introduction into MFI. Independent of the method of Zn introduction, all authors report Zn^{2+} cations present as either Zn^{2+} cations bridging two exchange sites (O−Zn^{2+}−O) or $[ZnOH]^+$ species. In addition, ZnO_x clusters and ZnO nanoparticles have been found in Zn/H-MFI prepared by sublimation of Zn, ZnO, $(CH_3)_2Zn$, and $ZnCl_2$, the last of which may also contain $[ZnCl]^+$ cations and/or zinc oxychloride species on the external surface of the zeolite crystals. Metallic Zn is reported only in the case of Zn sublimation. It is notable that the effects of Zn/Al loading on the species of Zn introduced have not been discussed, except in the case of aqueous ion exchange of $Zn(NO_3)_2$ into Na-MFI.[12]

A number of investigators have also sought to determine which Zn species are the most active for light alkane dehydrogenation and aromatization. Since alkane dehydrogenation limits the overall rate of light alkane dehydroaromatization over Zn/H-MFI, most of this work has focused on identifying the activity of different Zn species for this step. Both bridging Zn^{2+} cations[10] and $[ZnOH]^+$ cations[12,15] are reported to be active for propane dehydrogenation and aromatization, whereas cationic ZnO_x aggregates with a nuclearity greater than two[13] and bulk-like ZnO clusters[10,13,15] are reported to be inactive for both reactions.[10,13,15] While binuclear cationic oxygenated Zn species, possibly in the form of Zn^{2+}−O−Zn^{2+} dimers, have been reported to be active for propane dehydrogenation,[13] it has been noted that the propane dehydrogenation and aromatization activities of Zn^{2+}−O−Zn^{2+} dimers and bridging Zn^{2+} sites are lower than that of $[ZnOH]^+$ cations.[12] Additionally, it has been recently reported that $[ZnOH]^+$ cations may convert to $[ZnH]^+$ cations upon exposure to H_2 at a high temperature (≳400 K).[30,31] The heterolytic dissociation of H_2 over Zn^{2+} cations, resulting in the formation of $[ZnH]^+$ cations, has been demonstrated theoretically[32] and experimentally[24,26,29,33−35] at 273−473 K as well. The catalytic activity of $[ZnH]^+$ sites for alkane dehydrogenation is debated.[30,31] While $[ZnH]^+$ cations are found to be more active for C_5H_{12} aromatization than $[ZnOH]^+$ cations,[30] density functional theory (DFT) calculations suggest that $[ZnH]^+$ cations are less active for C_4H_{10} dehydrogenation compared to bridging Zn^{2+} or $[ZnOH]^+$ cations.[31]

The lack of clarity regarding the effect of the Zn/Al ratio on the Zn speciation and catalytic performance of Zn/H-MFI for light alkane dehydrogenation has motivated us to investigate this question for a single method of Zn/H-MFI preparation. In this work, we have prepared Zn/H-MFI catalysts with a range of Zn/Al ratios via solid-state ion exchange (SSIE) with $ZnCl_2$. We chose this preparation method because SSIE results in degrees of exchange that can exceed those obtained via conventional exchange procedures using aqueous media,[36] for which the maximum degree of Zn^{2+} exchange is determined by the availability of proximate Al atoms to charge-compensate for the divalent cations.[37] Zn speciation was characterized as a function of Zn loading using Fourier transform infrared spectroscopy (FTIR) of adsorbed pyridine, ^{27}Al and ^{1}H MAS NMR, UV−visible diffuse reflectance spectroscopy (UV−vis DRS), and X-ray absorption spectroscopy (XAS). The kinetics of propane dehydrogenation and cracking were then investigated for Zn/H-MFI with different Zn loadings. We also investigated the effects of adding H_2 to the feed on Zn speciation and the kinetics of C_3H_8 dehydrogenation and cracking.

2. EXPERIMENTAL METHODS

2.1. Synthesis of Zn/H-MFI Catalysts. NH_4-MFI zeolite (CBV 3024E) was obtained from Zeolyst International. H-MFI zeolite was prepared by loading approximately 1.0−1.25 g of NH_4-MFI into a quartz boat that was placed inside a quartz tube and then heated to 773 K at 2 K min^{-1} in 100 mL min^{-1} of flowing synthetic air (Praxair, Ultra Zero). The samples were held at 773 K for 4 h to convert the NH_4-MFI to the H^+ form. The H-MFI has a Si/Al ratio of 16.5 ± 1.0, as determined by ICP-OES measurements performed by Galbraith Laboratories (Knoxville, TN).[6] This parent H-MFI zeolite is denoted H-MFI (P).

Zn/H-MFI was prepared by solid-state ion exchange (SSIE) of H-MFI with $ZnCl_2$. Prior to SSIE, the parent H-MFI was dehydrated by loading approximately 2 g of H-MFI (P) into a 10 mL glass ampule, which was then heated in a sand bath at 573 K for 3 h while under dynamic vacuum maintained via a Schlenk line. H-MFI dehydrated in this manner is denoted H-MFI (D). After dehydration, the ampule was sealed under N_2 and cycled into a N_2-purged glovebox. The dehydrated H-MFI was mixed with anhydrous $ZnCl_2$ (≥98%, Sigma-Aldrich) inside the glovebox using a mortar and pestle. The mixture of H-MFI and $ZnCl_2$ was then loaded into a new ampule, sealed under N_2, and removed from the glovebox. The ampule was submerged in liquid N_2 to prevent loss of Zn due to sublimation of $ZnCl_2$, and the ampule was then flame-sealed under dynamic vacuum on a Schlenk line. SSIE was carried out by heating the ampule in a quartz tube to 788 K at 5 K min^{-1} in 100 mL min^{-1} of flowing He (Praxair, 99.999%) and then holding at 788 K for 2 h.

2.2. Catalyst Characterization. The Zn and Al contents of Zn/H-MFI samples were measured by Galbraith Labo-

https://doi.org/10.1021/acscatal.1c03641
ACS Catal. 2021, 11, 14489−14506

ratories using inductively coupled plasma optical emission spectroscopy (ICP-OES). The Cl content of samples was measured by Galbraith Laboratories using potentiometric titration. Powder X-ray diffraction (XRD) patterns of H-MFI and Zn/H-MFI were acquired using a Bruker D8 GADDS diffractometer equipped with a Cu-Kα source (40 kV, 40 mA). N_2 adsorption isotherms were acquired at 77 K using a Micrometrics Gemini VII surface area and porosity instrument. Prior to measurement of N_2 adsorption isotherms, 50 mg samples of H-MFI and Zn/H-MFI were degassed overnight at 423 K using a Micrometrics VacPrep 061. Micropore volumes were calculated using the t-plot method.

Infrared spectra of H-MFI and Zn/H-MFI were acquired using a Nicolet 6700 FTIR spectrometer with a liquid nitrogen-cooled Hg−Cd−Te (MCT) detector. Self-supporting pellets of H-MFI and Zn/H-MFI were prepared using 30−50 mg of catalyst. Pellets were placed in a stainless steel sample holder and loaded into an in situ transmission IR cell with CaF_2 windows. Prior to acquisition of FTIR spectra, samples were heated to 573 K at 5 K min^{-1} under 100 mL min^{-1} of flowing He (Praxair, 99.999%). The samples were held at 573 K for 2 h and then cooled to 473 K for acquisition of spectra. The samples were then cooled to 393 K, and pyridine was introduced into the flowing He using a syringe. Spectra were acquired after stabilization of the adsorbed pyridine, approximately 20−30 min after pyridine introduction. Baseline correction was performed using a spline function, and spectra were normalized to the integrated intensity of zeolite framework vibrational overtones in the region of 1700−2100 cm^{-1}. Additionally, FTIR spectra of H-MFI, and FTIR spectra pyridine adsorbed on H-MFI, were acquired after sample heating at 773 K for 1 h. As shown in Figure S1, similar results are obtained for catalysts heated at 773 K compared to those at 573 K. However, Zn/H-MFI samples were heated at 573 K prior to IR measurements to maintain a pretreatment temperature consistent with that used for ^{1}H MAS NMR and UV−visible diffuse reflectance spectroscopy experiments (described below), facilitating comparison between results obtained using different spectroscopic techniques. The Schlenk line vacuum dehydration setup and high-temperature reaction chamber used for ^{1}H MAS NMR and UV−visible diffuse reflectance spectroscopy experiments, respectively, did not allow for sample heating at temperatures above ∼573 K. As described in the discussion of our XAS results, samples heated at 773 K differ from those heated at 573 K only in that the latter samples may contain a slightly lower Cl content.

^{1}H MAS NMR and ^{1}H−^{27}Al TRAPDOR NMR spectra of H-MFI and Zn/H-MFI were acquired using a Bruker AV-700 NMR spectrometer equipped with a 3.2 mm probe and using a spinning frequency of 20 kHz. Samples (∼100 mg) were dehydrated by heating in a sand bath at 573 K for 3 h under dynamic vacuum using a Schlenk line and then transferred to a N_2-purged glovebox and loaded into a ZrO_2 rotor. ^{1}H MAS NMR spectra were obtained using a Hahn-Echo pulse sequence with a 90° pulse duration of 3.75 μs. The delay between scans was 5 s. One hundred and twenty-eight scans were averaged to produce the final spectrum of H-MFI, and 256 scans were averaged to produce the final spectra of Zn/H-MFI. Chemical shifts were referenced to tetramethylsilane (TMS). ^{1}H−^{27}Al TRAPDOR NMR spectra were obtained using a Hahn-Echo pulse sequence with delays τ of 7 rotor periods and ^{27}Al irradiation during the period τ between the 90 and 180° pulses. Two hundred and fifty-six scans were averaged to produce the final spectra. ^{27}Al MAS NMR spectra of H-MFI and Zn/H-MFI were acquired using a Bruker AV-700 NMR spectrometer. The samples (70−90 mg) were hydrated prior to measurement. Spectra were acquired using a 3.2 mm probe with a spinning frequency of 10 kHz and a pulse length of 0.78 μs (corresponding to a 15° flip angle). A total of 8192 scans were averaged to produce the final spectra. Chemical shifts were referenced to a 1 M aqueous solution of $Al(NO_3)_3$, and spectra are normalized by the maximum intensity in each spectrum.

UV−visible diffuse reflectance spectra (UV−vis DRS) were acquired using a Thermo Scientific Evolution 300 UV−visible spectrophotometer equipped with a Praying Mantis diffuse reflectance accessory (Harrick). Samples were loaded into a Praying Mantis high-temperature reaction chamber (Harrick) and heated to 573 K at 10 K min^{-1} under 100 mL min^{-1} of flowing He (Praxair, 99.999%). The samples were held at 573 K for 1 h and then cooled to ambient temperature for acquisition of spectra. Absorption intensities were calculated from the reflectance data using the Kubelka−Munk equation. The diffuse reflectance R_∞ is defined here as the reflectance of the Zn/H-MFI sample divided by the reflectance of H-MFI. H-MFI provided a relevant reference to emphasize the effects of Zn incorporation into the zeolite.

Zn K-edge X-ray absorption spectroscopy (XAS) was performed at Beamline 10-BM-A,B at the Advanced Photon Source at Argonne National Laboratory. XAS measurements were performed in transmission mode, and the monochromator energy was calibrated using Zn foil, which was measured simultaneously with the samples. The edge energy of Zn foil was set to 9659.0 eV. ZnO (Sigma-Aldrich) and $ZnCl_2$ (Sigma-Aldrich) standards were sealed in Kapton tape for XAS measurements at ambient conditions. Zn/H-MFI samples of varying Zn loadings were pressed into self-supporting pellets and loaded into a stainless steel 6-shooter sample holder. The sample holder was placed in a quartz tube equipped with Kapton windows and a gas inlet and outlet. Gases were metered to the sample holder using digital mass flow controllers. XAS spectra of as-prepared, hydrated Zn/H-MFI samples were initially acquired in air at ambient temperature. Zn/H-MFI samples were subsequently heated to 573 K at 5 K min^{-1} in 100 mL min^{-1} of flowing He (Airgas), and XAS spectra were acquired. Zn/H-MFI samples were then heated to 773 K at 5 K min^{-1} in flowing He, and XAS spectra were acquired. The gas flow was then switched to 100 mL min^{-1} of 3% H_2 in He (Airgas) at 773 K, and the samples were held at these conditions for 6 h prior to acquisition of XAS spectra.

Athena software was used for normalization of XAS spectra and background subtraction to extract the EXAFS spectra $\chi(E)$.[38] The EXAFS spectra of Zn/H-MFI were Fourier-transformed in the range of 2.5−10 Å^{-1} in k-space using a Hanning window with 1 Å sills. Multiple k-weight (k, k^2, and k^3) fitting of the first coordination shell of Zn, which was modeled with O and Cl backscatterers, was performed in the range of 1−2.4 Å in R-space using Artemis software.[38] All of the EXAFS spectra of the Zn/H-MFI samples were fit simultaneously using a single inner potential correction $\Delta E_{0,O}$ for all Zn−O scattering paths and a single inner potential correction $\Delta E_{0,Cl}$ for all Zn−Cl scattering paths. The first coordination shell of a Zn metal standard was also fit simultaneously to obtain the amplitude reduction factor S_0^2. The scattering amplitudes and phase shifts for Zn−Cl and Zn−

https://doi.org/10.1021/acscatal.1c03641
ACS Catal. 2021, 11, 14489−14506

O scattering paths were calculated from the crystal structures of $ZnCl_2$ and ZnO, respectively, in Artemis using FEFF6.

2.3. Measurements of C_3H_8 Dehydrogenation and Cracking. The rates of propane dehydrogenation and cracking over H-MFI and Zn/H-MFI were measured using a tubular quartz reactor (6.5 mm o.d.) containing 15 mg of catalyst supported on quartz wool. The reactor was heated using a cylindrical furnace, and the reactor temperature was controlled using a CN7500 temperature controller (Omega) and a K-type thermocouple (Omega) placed outside the reactor next to the catalyst bed. Gases were metered to the reactor using digital mass flow controllers (Brooks Instrument) that were first calibrated using a bubble flowmeter.

Prior to measuring reaction rates, catalyst samples were heated to 773 K at 5 K min^{-1} in 100 mL min^{-1} of flowing synthetic air (Praxair, Ultra Zero) and held at this temperature for 1 h. The reactor was then purged with 100 mL min^{-1} of flowing He (Praxair, 99.999%) for 10 min at 773 K. Next, the gas flow was switched to 100 mL min^{-1} of flowing 2.5% H_2 in He (Praxair, CSG) at 773 K, and the samples were held under these conditions for 7 h. The gas flow was then switched to 100 mL min^{-1} of flowing He (Praxair, 99.999%), and the temperature was lowered to 733 K. Samples were held at these conditions overnight.

For reaction rate measurements, the partial pressure of C_3H_8 in the reactor feed was varied by diluting 2.5% C_3H_8/He (Praxair, CSG) or 20% C_3H_8/He (Praxair, CSG) with He (Praxair, 99.999%) to obtain C_3H_8 partial pressures varying from 0.8 to 4.5 kPa. The flowrates of the C_3H_8/He and He streams were varied to obtain space times ranging from 7 to 22 mol Al·s/mol C_3H_8 for each inlet C_3H_8 partial pressure. For experiments in which H_2 was cofed, 2.5% H_2/He (Praxair, CSG) was mixed with 2.5% C_3H_8/He and He to obtain a H_2 partial pressure of 0.5 kPa and a C_3H_8 partial pressure of 0.8 kPa. The reaction products were analyzed using a Varian CP-3800 gas chromatograph containing a Varian CP-Al_2O_3/Na_2SO_4 capillary column (5 μm, 0.32 mm i.d. × 50 m) and equipped with a flame ionization detector (FID). FID response factors were determined using a gas mixture containing known quantities of CH_4, C_2H_6, C_2H_4, C_3H_8, C_3H_6, n-C_4H_{10}, 1-C_4H_8, cis-2-C_4H_8, trans-2-C_4H_8, and n-C_5H_{12}. The mixture was diluted with He to obtain a range of inlet hydrocarbon partial pressures.

Product formation rates and carbon selectivities during C_3H_8 conversion over H-MFI and Zn/H-MFI were measured at differential conversion (<9% C_3H_8 conversion) at temperatures ranging from 713 to 773 K. For each combination of C_3H_8 inlet partial pressure and reaction temperature investigated, rate measurements were performed at four different space times. Product formation rates and carbon selectivities were extrapolated linearly to zero space time to remove the effects of secondary reactions and product inhibition on the reaction kinetics. The rate of CH_4 formation extrapolated to zero space time was nearly equal to that of C_2H_4 formation. The rate of C_3H_8 cracking was therefore taken to be the rate of formation of either product extrapolated to zero space time. The rate of C_3H_8 dehydrogenation was taken to be the rate of C_3H_6 formation extrapolated to zero space time.

3. RESULTS AND DISCUSSION

3.1. Catalyst Characterization. The Zn/Al and Cl/Zn ratios of as-prepared and spent (treated in 2.5% H_2 in He at 773 K and then used for studies of C_3H_8 dehydrogenation and cracking) Zn/H-MFI catalysts are given in Table 2. For all Zn weight loadings, the Cl/Zn ratio of as-prepared catalysts is comparable to that of the $ZnCl_2$ precursor, indicating that significant amounts of Cl are retained in the catalyst after solid-state ion exchange. However, near-complete removal of Cl from Zn/H-MFI samples of lower Zn loadings occurred after treatment in 2.5% H_2 in He and exposure to C_3H_8 conversion reaction conditions. Zn is also lost from all Zn/H-MFI samples during this treatment, the percentage generally increasing with the Zn/Al ratio of the as-prepared sample. The micropore volumes of the Zn/H-MFI catalysts and of the parent zeolite H-MFI (P) and of H-MFI dehydrated under dynamic vacuum, i.e., H-MFI (D), are given in Table 2 as well. H-MFI (P) and H-MFI (D) exhibit similar micropore volumes. SSIE with $ZnCl_2$ causes a decrease in the micropore volume due to the presence of Zn in the zeolite channels, but no trend in the micropore volume with the Zn/Al ratio was observed.

Table 2. Chemical and Textural Characterization of H-MFI and As-Prepared and Spent[a] Zn/H-MFI Catalysts

zeolite	Zn/Al (as-prepared)	Zn/Al (spent)	Cl/Zn (as-prepared)	Cl/Zn (spent)	micropore volume (as-prepared) [$cm^3\ g^{-1}$]
H-MFI (P)					0.12
H-MFI (D)					0.11
Zn/H-MFI	0.06	0.06	1.91	<0.05	0.07
	0.15	0.09	2.14	0.09	0.08
	0.23	0.13	1.16	0.07	0.07
	0.34	0.18	2.28		0.08
	0.52	0.24	1.69		0.07
	0.79	0.38	1.59	0.73	0.07
	0.94	0.36	1.57		0.08

[a]Spent catalysts were treated in 2.5% H_2 in He at 773 K for 7 h and then used for reaction rate measurements of C_3H_8 dehydrogenation and cracking over Zn/H-MFI.

XRD patterns of Zn/H-MFI with varying Zn weight loadings are shown in Figure S2, along with the XRD pattern of the parent H-MFI zeolite. The XRD patterns of the Zn/H-MFI catalysts confirm that the MFI structure is preserved following SSIE of $ZnCl_2$. The decrease in the relative intensities of the peaks at 7.9 and 8.8° with increasing Zn weight loading is attributed to the exchange of cationic Zn species for Brønsted acid protons.[39,40] The absence of peaks at 2θ angles of 32, 34, 37, and 47°, characteristic of ZnO in the wurtzite structure,[41] in the XRD patterns of Zn/H-MFI indicates that SSIE does not lead to the formation of X-ray-observable clusters of ZnO. The absence of diffraction peaks at 36 and 43° for Zn metal[40] in the XRD pattern of Zn/H-MFI indicates that X-ray-detectable clusters of Zn metal are not present in any of these catalyst samples. Finally, the absence of characteristic peaks of $ZnCl_2$ at 2θ angles of 16, 17, 26, 30, 36, 39, and 49°[42] indicates that Zn/H-MFI catalysts do not contain XRD-observable clusters of unexchanged $ZnCl_2$.

Fourier transform infrared spectroscopy (FTIR), FTIR of adsorbed pyridine (FTIR-py), and ^{1}H magic-angle spinning nuclear magnetic resonance (^{1}H MAS NMR) were used to probe the acid sites in Zn/H-MFI catalysts. FTIR spectra of Zn/H-MFI catalysts, as well as the spectra of H-MFI (P) and

https://doi.org/10.1021/acscatal.1c03641
ACS Catal. 2021, 11, 14489−14506

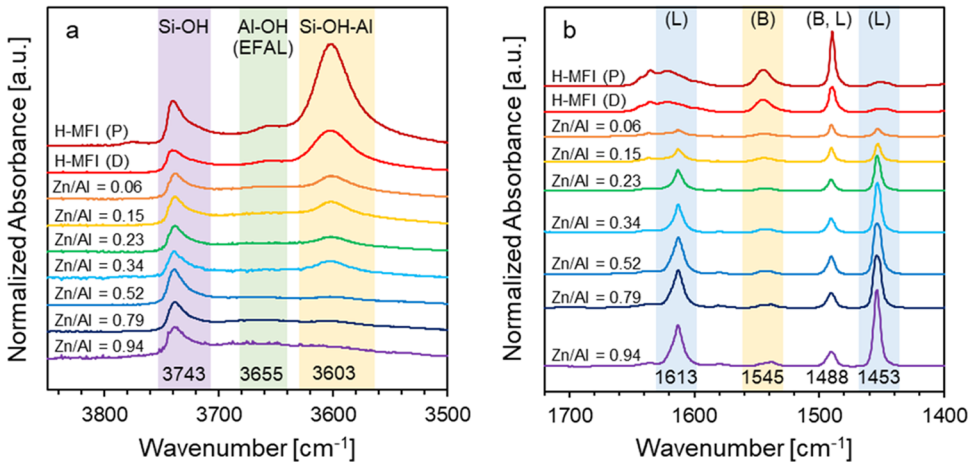

Figure 1. (a) Infrared spectra of H-MFI and Zn/H-MFI (Zn/Al = 0.06−0.94 in as-prepared samples). Spectra were acquired at 473 K under flowing He. (b) Infrared spectra of pyridine adsorbed on H-MFI and Zn/H-MFI (Zn/Al = 0.06−0.94 in as-prepared samples). Pyridine adsorption was performed, and spectra were acquired at 393 K under flowing He.

H-MFI (D), are shown in Figure 1a. The FTIR spectrum of H-MFI (P) exhibits a band at 3603 cm^{-1} corresponding to the stretching vibration of Brønsted acid OH groups, a band at 3655 cm^{-1} corresponding to the stretching vibration of Al−OH groups associated with extraframework Al atoms, and a band at 3743 cm^{-1} corresponding to the stretching vibration of Si−OH groups at defect sites in zeolite pores or on the external surface of zeolite crystallites.[43,44]

As shown in the FTIR spectrum of H-MFI (D), the intensities of the bands at 3603 and 3743 cm^{-1} decrease significantly after dehydration under dynamic vacuum, likely due to partial dehydroxylation of the zeolite framework.[29,45] While the mechanism of zeolite dehydroxylation is not well understood, it has been proposed that in the vicinity of a defect site, a Brønsted acid OH group can recombine with a Si−OH group, releasing water and resulting in the formation of a three-coordinate Al atom.[45] Alternatively, a Brønsted acid OH group in the vicinity of a defect site on an Al atom may be dehydroxylated under vacuum in the absence of a neighboring Si−OH group, also resulting in the formation of a three-coordinate Al atom. The three-coordinate Al atoms are, however, not stable when exposed to room-temperature air; dissociation of water molecules at the Al atoms allows them to adopt an octahedral coordination.[45] Two Brønsted acid OH groups may also be dehydroxylated under vacuum to form water, three-coordinate Al, and four-coordinate Al.[29] Compared to the corresponding bands in H-MFI (P), the fractional decrease in the intensity of the band attributed to Brønsted acid OH groups in H-MFI (D) may be larger than that of the band attributed to Si−OH groups. Thus, dehydroxylation of H-MFI (P) is proposed to occur, in part, via recombination of Brønsted OH and Si−OH groups and partially in the absence of a neighboring Si−OH group. However, dehydroxylation of H-MFI (P) is not followed by dealumination of the zeolite, as evidenced by the absence of an increase in the intensity of the band at 3655 cm^{-1} and confirmed by ^{1}H and ^{27}Al MAS NMR (see below).

FTIR spectra of Zn/H-MFI catalysts exhibit a decrease in the intensity of the band at 3603 cm^{-1} with increasing Zn loading, although the low band intensity (relative to H-MFI (P)) at low Zn/Al ratios is primarily due to dehydroxylation of the zeolite framework, which occurs in all samples during dehydration of the parent H-MFI and during SSIE. The intensity of the band at 3743 cm^{-1} remains approximately constant as the Zn/Al ratio is increased. These observations suggest that Zn is primarily exchanged at the Brønsted acid sites, rather than at Si−OH groups. However, this process does not release HCl, as would be expected, since the Cl/Zn ratio remains between 1.6 and 2.0 after reaction of H-MFI with $ZnCl_2$ (see Table 2). An explanation of how this may occur is given below as a part of the discussion of our EXAFS results.

FTIR of adsorbed pyridine was used to probe the Brønsted and Lewis acidities of as-prepared Zn/H-MFI. FTIR-py spectra of H-MFI (P), H-MFI (D), and Zn/H-MFI catalysts are shown in Figures 1b and S3. The spectra exhibit bands at 1453 and 1545 cm^{-1}, attributed to ring vibrations of pyridine adsorbed on Lewis acid sites and on Brønsted acid sites, respectively.[46] Consistent with the FTIR results discussed previously, FTIR-py spectra of H-MFI (D) exhibit a decrease in the intensity of the band at 1545 cm^{-1} relative to the corresponding band in H-MFI (P), indicating a lower Brønsted acid site content in H-MFI (D) relative to H-MFI (P) due to partial dehydroxylation of the zeolite framework. The intensity of the band at 1545 cm^{-1} is significantly attenuated in Zn/H-MFI (Zn/Al = 0.06) relative to H-MFI (P) and H-MFI (D) and remains approximately constant as the Zn/Al ratio increases, consistent with FTIR results. The constant, low band intensity may indicate that the vast majority of Brønsted acid sites, with the exception of those in the vicinity of exchanged Zn species, have been dehydroxylated. This is consistent with previous work suggesting that zeolite framework Al atoms near exchanged Zn species are stable to dealumination via steaming.[47] As shown in Figure 2, the FTIR-py spectra of Zn/H-MFI exhibit an approximately linear increase in the integrated intensity of the band at 1453 cm^{-1} as the Zn/Al ratio increases from 0.06 to 0.52, suggesting that only isolated Zn Lewis acid sites are present at these Zn loadings. At higher Zn/Al ratios, multinuclear clusters of Zn-containing species may form, which could explain why the intensity of the band at 1453 cm^{-1} no longer increases with increasing Zn/Al ratio.

The FTIR-py spectra also exhibit a band at 1488 cm^{-1}, which contains contributions from pyridine adsorbed on both Brønsted and Lewis acid sites. The intensity of this band is lower for H-MFI (D) and Zn/H-MFI (Zn/Al = 0.06) compared to that for H-MFI (P) due to dehydroxylation of

https://doi.org/10.1021/acscatal.1c03641
ACS Catal. 2021, 11, 14489−14506

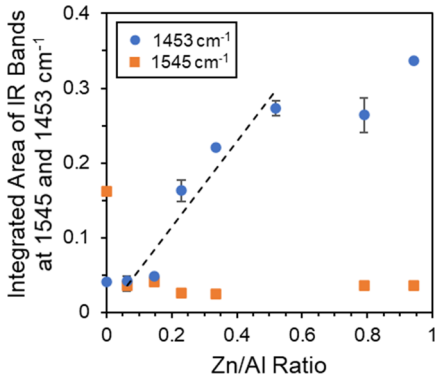

Figure 2. Effect of the Zn/Al ratio of Zn/H-MFI (Zn/Al = 0.06−0.94 in as-prepared samples) on the intensity of the IR bands at 1453 cm^{-1} (corresponding to Lewis acid sites) and 1545 cm^{-1} (corresponding to Brønsted acid sites) for pyridine adsorbed on Zn/H-MFI. Pyridine adsorption was performed, and spectra were acquired at 393 K under flowing He.

the zeolite framework in the former samples. As the Zn/Al ratio increases, the change in the integrated intensity of this band parallels that of the band at 1453 cm^{-1}. Finally, FTIR-py spectra exhibit a band at 1613 cm^{-1} that arises from pyridine adsorbed on Lewis acid sites. The position of this band, which is indicative of Lewis acid strength, does not vary with Zn loading, suggesting that there is no significant variation in the strength of the Lewis acid sites across Zn/H-MFI samples.

^{1}H MAS NMR was used to further probe the nature of OH groups in Zn/H-MFI catalysts. ^{1}H MAS NMR spectra of H-MFI and Zn/H-MFI catalysts are shown in Figure 3a. The spectrum of H-MFI (D) exhibits a signal at 4.4 ppm attributed to Brønsted acid OH groups, a signal 2.5 ppm attributed to Al−OH groups associated with extraframework Al atoms, and a signal at 1.8 ppm attributed to Si−OH groups at the external surface of zeolite crystallites or at defect sites.[48] A signal at 0.2 ppm is also detected in H-MFI (D) and Zn/H-MFI. In agreement with the FTIR results, the intensity of the signal at 4.0−4.4 ppm in Zn/H-MFI is significantly attenuated relative to the intensity of the corresponding signal in H-MFI (D), and the intensity of the signal at 1.8 ppm is attenuated to a lesser extent. These changes are consistent with dehydroxylation of the zeolite framework and reaction of Zn primarily with Brønsted acid sites and not with Si−OH groups. Additionally, the intensity of the signal at 2.5 ppm is largely unchanged in Zn/H-MFI relative to H-MFI, except in Zn/H-MFI with a Zn/Al ratio of 0.94. The absence of an increase in the intensity of this signal suggests that the zeolite is not dealuminated upon SSIE. Al−OH groups have, however, been consumed in Zn/H-MFI (Zn/Al = 0.94). Furthermore, as the Zn content of Zn/H-MFI catalysts is increased, the intensity of the signal at 0.2 ppm appears to increase slightly. ^{1}H−^{27}Al TRAPDOR NMR (discussed in Section S.4) shows that this signal may arise from Zn−OH groups or may be due to a metal impurity. Finally, ^{1}H MAS NMR spectra of H-MFI, Zn/H-MFI (Zn/Al = 0.06), and Zn/H-MFI (Zn/Al = 0.94) also exhibit a broad signal arising from small amounts of physisorbed water, overlapping with the signal due to Brønsted acid OH groups;[49] it is possible that atmospheric moisture entered the NMR rotor after these samples were loaded. However, it remains apparent that the signal in the region of 4 ppm is significantly smaller for these Zn/H-MFI samples compared to that for H-MFI (D), confirming our FTIR results.

^{27}Al MAS NMR was used to probe for dealumination occurring during dehydration of H-MFI under vacuum or solid-state ion exchange with $ZnCl_2$. ^{27}Al MAS NMR spectra of H-MFI and Zn/H-MFI are shown in Figure 3b. In the spectra of H-MFI (P) and H-MFI (D), signals are observed at 51 and 0 ppm. These signals are attributed to tetrahedrally coordinated Al atoms in the zeolite framework and to octahedrally coordinated extraframework Al atoms, respectively.[50] The relative intensities of these two signals are the same in both spectra, indicating that dehydration of H-MFI under dynamic vacuum does not cause dealumination of the framework, which would result in an increase in the intensity of the signal at 0 ppm. Additionally, in the spectra of Zn/H-MFI with Zn/Al ratios of 0.06−0.34, a broad signal in the range of 20−40 ppm is observed, and its intensity increases with increasing Zn content. The relative intensity of the signal at 0 ppm increases as well, which may be attributed to dehydroxylation of the zeolite framework, as discussed previously. A similar change in ^{27}Al MAS NMR spectra of samples of desilicated zeolite Y has been previously observed after calcination at 770 K and was attributed to dehydroxylation.[51] In the spectrum of Zn/H-MFI with a Zn/Al ratio of 0.94, a broad signal at 10−15 ppm is observed. From the 1D ^{27}Al MAS NMR spectra, it is not possible to determine whether these signals are due to five-coordinate Al atoms or

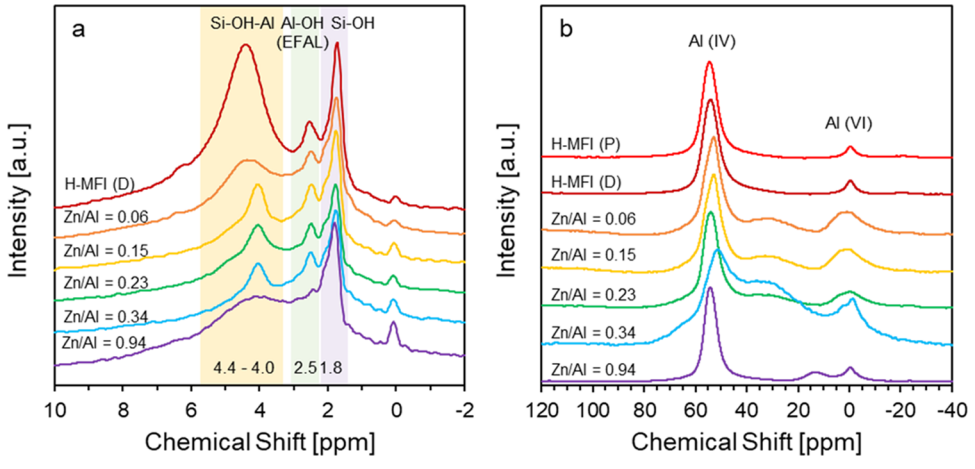

Figure 3. (a) ^{1}H MAS NMR and (b) ^{27}Al MAS NMR spectra of H-MFI and Zn/H-MFI (Zn/Al = 0.06−0.94 in as-prepared samples).

https://doi.org/10.1021/acscatal.1c03641
ACS Catal. 2021, 11, 14489−14506

alternatively to tetrahedrally or octahedrally coordinated Al atoms; the peak position and width of ^{27}Al MAS NMR signals are affected by quadrupolar interactions.[52] However, it is likely that the signals in the range of 20−40 ppm are associated with framework Al atoms in the vicinity of exchanged Zn species. It is possible that the signal at 10−15 ppm arises from $ZnAl_2O_4$[53,54] or $ZnAl_2O_{4-x}Cl_{2x}$ nanoclusters (see Section S.5). The formation of $ZnAl_2O_4$/$ZnAl_2O_{4-x}Cl_{2x}$ nanoclusters is consistent with the FTIR-py results shown in Figure 2; based on those results, it is likely that $ZnAl_2O_4$/$ZnAl_2O_{4-x}Cl_{2x}$ nanoclusters are also present in Zn/H-MFI (Zn/Al = 0.79). This could account for the significant retention of Cl in the spent catalyst (see Table 2). The $ZnAl_2O_4$/$ZnAl_2O_{4-x}Cl_{2x}$ nanoclusters are insufficiently large or crystalline such that they cannot be identified by XRD; the XRD pattern of Zn/H-MFI with a Zn/Al ratio of 0.94 does not exhibit the characteristic peaks of $ZnAl_2O_4$ at 2θ angles of 32 and 36°.[54,55]

As noted earlier, XRD gave no evidence of diffraction peaks for the presence of ZnO nanoparticles in Zn/H-MFI. Therefore, we used UV−visible diffuse reflectance spectroscopy (UV−vis DRS) to look for evidence of ZnO nanoparticles. Figure 4a shows UV−vis DRS spectra of Zn/H-MFI catalysts.

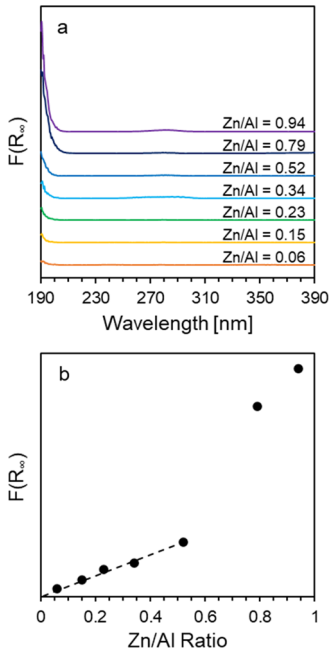

Figure 4. (a) UV−visible diffuse reflectance spectra of Zn/H-MFI (Zn/Al = 0.06−0.94 in as-prepared samples) and (b) maximum absorbance as a function of Zn loading.

The spectra exhibit an absorption band in the region below 210 nm, attributed to ligand-to-metal charge transfer from O^{2-} in the zeolite framework to isolated Zn^{2+} species.[56] The maximum absorbance, shown as a function of Zn/Al in Figure 4b, increases linearly with increasing Zn loading for Zn/Al = 0.06−0.52. This suggests that as the Zn loading increases within this range, an increasing quantity of Zn species with identical ligand-to-metal charge-transfer characteristics is formed. Zn/H-MFI does not contain ZnO, as demonstrated by the absence of an absorption onset at 265 or 375 nm, corresponding to subnanometric ZnO confined in zeolite channels or macrocrystalline ZnO on the external surface of the zeolite, respectively.[57] However, as discussed in Section S.5, UV−vis DRS spectra indicate that $ZnAl_2O_4$ or $ZnAl_2O_{4-x}Cl_{2x}$ nanoclusters may be present in Zn/H-MFI catalysts with high Zn loadings.

XAS at the Zn K-edge was used to investigate the effects of Zn loading and postsynthetic treatment on the nature of Zn species in Zn/H-MFI. X-ray absorption near-edge spectra (XANES) of hydrated Zn/H-MFI, acquired under ambient conditions, are shown in Figure 5a. XANES spectra of Zn/H-MFI (Zn/Al = 0.34) during postsynthetic treatment in He at temperatures up to 773 K, and subsequently in 2.5% H_2 in He at 773 K, are shown in Figure 5b. These results are qualitatively similar for all Zn loadings measured, as shown in Figures S8−S10. XANES spectra of $ZnCl_2$, ZnO, and Zn metal standards, acquired under ambient conditions, are also shown in Figure 5a. The Zn K-edge energy, which is defined here as the zero-crossing of the second derivative of the unnormalized absorption, of the Zn/H-MFI samples and the standards is reported in Table 3. The Zn K-edge energy of Zn/H-MFI (9662.5−9663.1 eV) is not influenced by Zn loading or postsynthetic treatment and is similar to those of Zn^{2+} standards (9661.4 eV for ZnO and 9662.7 eV for $ZnCl_2$), indicating that Zn is present predominantly as Zn^{2+} cations. Moreover, the overall shape of the XANES spectra of hydrated Zn/H-MFI samples is similar to that of hydrated Zn/H-MFI prepared by chemical vapor deposition of dimethylzinc, which contains isolated, four- or five-coordinate Zn species.[13] Comparison with XANES spectra of standards also suggests that bulk ZnO, $ZnCl_2$, or Zn metal is not present in hydrated Zn/H-MFI or in Zn/H-MFI during postsynthetic treatment. Interestingly, the XANES spectrum of Zn/H-MFI (Zn/Al = 0.94) does not appear to contain contributions from $ZnAl_2O_4$ or $ZnAl_2O_{4-x}Cl_{2x}$ nanoclusters.[58] This may be because XAFS data provide an average over all Zn environments, and $ZnAl_2O_4$ or $ZnAl_2O_{4-x}Cl_{2x}$ nanoclusters are likely a minor fraction of all Zn species, as discussed in Section S.6.

The local coordination environment of Zn^{2+} cations in Zn/H-MFI was further analyzed using EXAFS. The Fourier transforms of the k^2-weighted EXAFS spectra (FT-EXAFS) of hydrated Zn/H-MFI samples and standards are shown in Figure 6 and those of Zn/H-MFI (Zn/Al = 0.34) during postsynthetic treatment in He at temperatures up to 773 K, and subsequently in 2.5% H_2 in He at 773 K, are shown in Figure 7. The dominant feature in the magnitude of the FT-EXAFS of Zn/H-MFI is a first-shell peak in the range of 1.0−2.0 Å (Figures 6a and 7a). Comparison with the FT-EXAFS of ZnO and $ZnCl_2$ suggests that the first-shell peak in the magnitude of the FT-EXAFS of Zn/H-MFI contains contributions from Zn−O and Zn−Cl backscattering. The magnitude of the FT-EXAFS of Zn/H-MFI samples at temperatures ≥573 K also exhibits a peak at ca. 2.5 Å (Figure 7a), arising from Zn−Al/Si backscattering.[59] EXAFS also confirms that Zn/H-MFI does not contain bulk Zn metal or ZnO. The magnitude of the FT-EXAFS of Zn metal exhibits a first-shell peak at ca. 2.3 Å due to Zn−Zn backscattering and that of ZnO exhibits a second-shell peak at ca. 2.9 Å due to backscattering from Zn next-nearest neighbors in Zn−O−Zn linkages (Figure 6a); these features are absent in the magnitude of the FT-EXAFS pattern for Zn/H-MFI.

The FT-EXAFS spectra of Zn/H-MFI were fit to determine the average number of O and Cl backscatterers in the first coordination shell, as well as their interatomic distances from Zn^{2+} cations. The fitted parameters are given in Table 4, and representative fits are shown in Figure S11 for Zn/H-MFI

https://doi.org/10.1021/acscatal.1c03641
ACS Catal. 2021, 11, 14489−14506

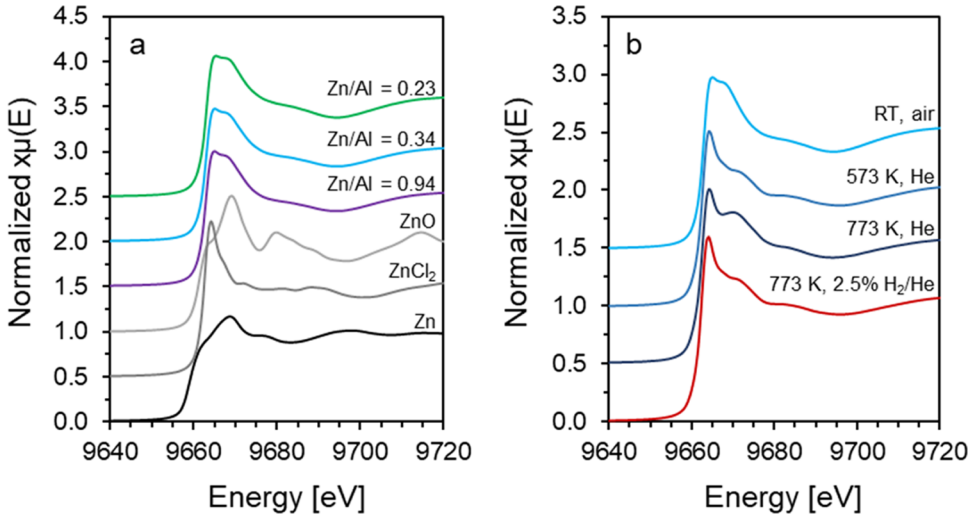

Figure 5. Normalized Zn K-edge X-ray absorption near-edge spectra (XANES) of Zn/H-MFI and Zn standards. (a) XANES spectra of Zn/H-MFI (Zn/Al = 0.23, 0.34, and 0.94 in as-prepared samples) at ambient conditions. XANES spectra of ZnO, $ZnCl_2$, and Zn metal standards at ambient conditions are also shown. (b) XANES spectra of Zn/H-MFI (Zn/Al = 0.34 in the as-prepared sample) at ambient conditions during treatment in He at 573 and 773 K and during treatment in 2.5% H_2/He at 773 K. The spectra are offset for clarity.

Table 3. Zn K-Edge Energies of Zn/H-MFI Samples and Standards

		Zn K-edge energy [eV]			
sample	Zn/Al	ambient conditions	573 K in He	773 K in He	773 K in 2.5% H_2/He
Zn metal		9659.0			
ZnO		9661.4			
$ZnCl_2$		9662.7			
Zn/H-MFI	0.23	9663.1	9662.7	9662.7	9662.7
	0.34	9663.0	9662.7	9662.6	9662.5
	0.94	9663.0	9662.7	9662.5	9662.5

(Zn/Al = 0.34). On average, Zn^{2+} centers in hydrated Zn/H-MFI are coordinated to 3.4−3.7 O neighbors at an interatomic distance of 1.99−2.00 Å and 1.3−1.5 Cl neighbors at an interatomic distance of 2.25−2.26 Å. This result is comparable to Cl/Zn ratios determined by ICP-OES and potentiometric titration (see Table 2). In the absence of bulk $ZnCl_2$, an average N_{Cl} in excess of one might be ascribable to the adsorption of HCl on Zn^{2+} species via interaction between the Cl of HCl and the Zn^{2+} center. It has been reported that HCl adsorbs in this configuration for Cu/H-MFI.[60] Furthermore, the adsorption of HCl has been proposed to account for Cl/Zn ratios greater than one in $ZnCl_2$-modified alumina, H-MFI, and H-BEA after methyl chloride synthesis from HCl and methanol.[61] It should be noted that while the adsorption of 0.1 μbar HCl on Cu/H-MFI gives rise to an IR band at 2160 cm^{-1},[60] no such feature was observed for as-prepared Zn/H-MFI. Additionally, ^{1}H MAS NMR spectra do not provide evidence of adsorbed HCl, although to the best of our knowledge, ^{1}H MAS NMR has not been previously used to probe HCl adsorption on zeolites, and ^{1}H MAS NMR spectra of HCl adsorbed on alumina exhibit only broad features.[62]

After treatment in He at 773 K, Zn^{2+} centers are coordinated to ∼2 O neighbors at an interatomic distance of 1.94 Å and an ∼1 Cl neighbor at 2.25−2.27 Å. The lower Zn−O coordination number and average interatomic distance are

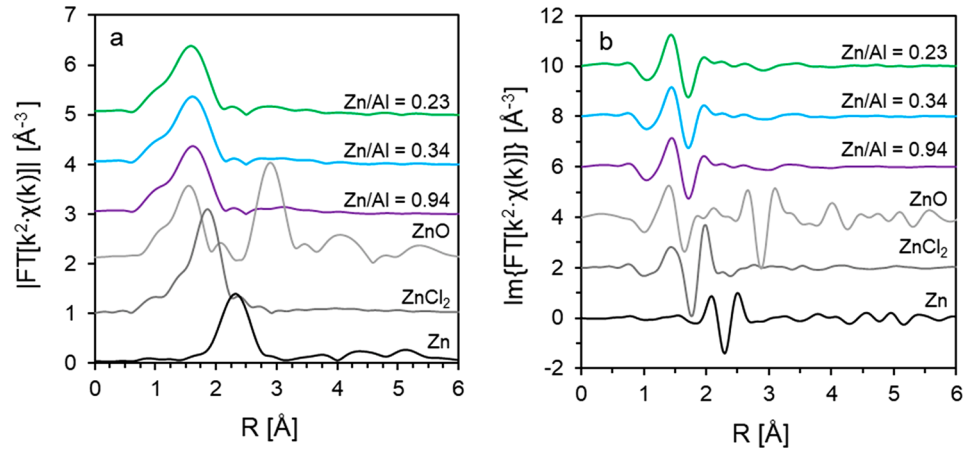

Figure 6. (a) Magnitude and (b) imaginary components of the Fourier-transformed k^2-weighted extended X-ray absorption fine structure spectra (EXAFS) of Zn/H-MFI (Zn/Al = 0.23, 0.34, and 0.94) at ambient conditions. EXAFS spectra of ZnO, $ZnCl_2$, and Zn metal standards at ambient conditions are also shown. The spectra are offset for clarity.

https://doi.org/10.1021/acscatal.1c03641
ACS Catal. 2021, 11, 14489−14506

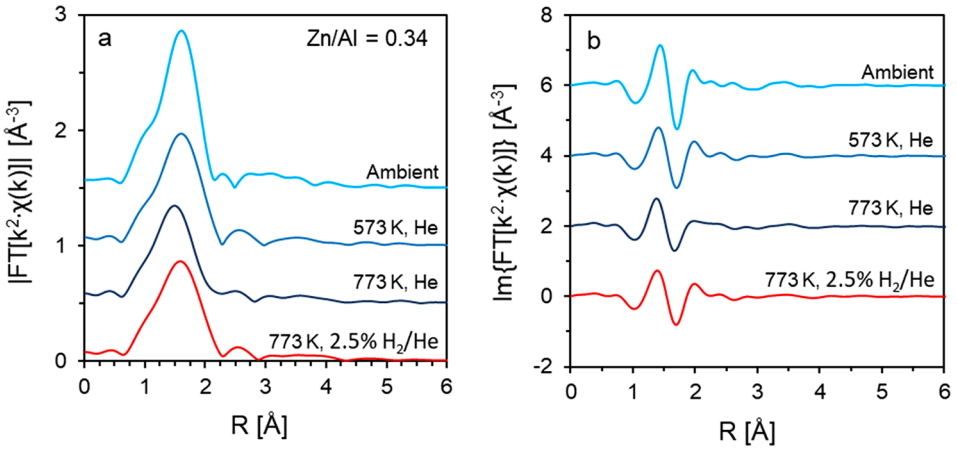

Figure 7. (a) Magnitude and (b) imaginary components of the Fourier-transformed k^2-weighted extended X-ray absorption fine structure spectra (EXAFS) of Zn/H-MFI (Zn/Al = 0.34) at ambient conditions during treatment in He at 573 and 773 K and during treatment in 2.5% H_2/He at 773 K. The spectra are offset for clarity.

Table 4. Fitted Parameters for Fourier-Transformed Zn K-Edge EXAFS of Zn/H-MFI Acquired at Ambient Conditions, 573 and 773 K in He, and 773 K in 2.5% H_2/He[a]

Zn/Al	sample conditions	N_O[b]	N_{Cl}[c]	total N	R_O[d] [Å]	R_{Cl}[e] [Å]	σ^2[f] [10^{-3} ·Å]
0.23	ambient	3.8	1.3	5.1	1.99	2.26	6.7
	573 K, He	2.1	0.8	2.9	1.98	2.27	4.8
	773 K, He	2.1	0.8	2.8	1.94	2.25	6.1
	773 K, 2.5% H_2/He	2.4	0.5	2.9	1.94	2.26	
0.34	ambient	3.4	1.5	4.9	2.00	2.25	6.7
	573 K, He	2.0	1.2	3.2	1.96	2.27	4.8
	773 K, He	2.0	0.9	2.9	1.94	2.27	6.1
	773 K, 2.5% H_2/He	2.3	0.7	3.0	1.94	2.28	
0.94	ambient	3.4	1.5	5.0	2.00	2.25	6.7
	573 K, He	1.9	1.5	3.3	1.95	2.28	4.8
	773 K, He	2.0	1.2	3.1	1.94	2.27	6.1
	773 K, 2.5% H_2/He	2.3	0.9	3.2	1.94	2.28	

[a] *R*-factor: 0.003. The amplitude reduction factor S_0^2 is 0.78 ± 0.14. The inner potential correction $\Delta E_{0,O}$ is 0.1 ± 0.8, and the inner potential correction $\Delta E_{0,Cl}$ is 3.6 ± 1.2. [b] The uncertainty in the coordination number N_O is ±0.8−0.9 for ambient conditions and ±0.4−0.5 for 573−773 K in He or 2.5% H_2 in He. [c] The uncertainty in the coordination number N_{Cl} is ±0.5 for ambient conditions and ±0.2−0.3 for 573−773 K in He or 2.5% H_2 in He. [d] The uncertainty in the interatomic distance R_O is ±0.01−0.02. [e] The uncertainty in the interatomic distance R_{Cl} is ±0.01−0.03. [f] The uncertainty in the Debye−Waller factor σ^2 is ±0.003 for ambient conditions and ±0.002 for 573−773 K in He or 2.5% H_2 in He.

consistent with the removal of adsorbed water. The loss of Cl upon high-temperature treatment in He may be due to the removal of adsorbed HCl. It should also be noted that although cationic Zn species in dehydrated zeolites are typically reported to exhibit fourfold coordination,[9] Schweitzer et al. have used EXAFS to show that SiO_2-supported Zn^{2+} cations are three-coordinate under propane dehydrogenation reaction conditions,[63] and Camacho-Bunquin et al. have used EXAFS to show that three-coordinate ethyl-zinc(II) species are formed when dimethylzinc is grafted on SiO_2.[64] Moreover, Mahyuddin et al. have shown from DFT calculations that three-coordinated Zn^{2+} cations in 8-member rings of MFI are active for methane activation.[65] A Zn−O interatomic distance of 1.94 Å is consistent with the previously reported value of 1.94 Å for three-coordinate Zn^{2+} species in ethyl-zinc on SiO_2.[64]

After treatment of Zn/H-MFI in 2.5% H_2 in He at 773 K, the Zn−O and Zn−Cl interatomic distances are unchanged, and there remains a total of three O and Cl atoms in the first coordination shell of Zn^{2+} centers. However, the average number of Cl neighbors appears to decrease slightly (N_{Cl} = 0.6−0.9) and the average number of O neighbors appears to increase slightly (N_O = 2.4), though due to the uncertainty associated with the fitted coordination numbers, we cannot determine conclusively that N_{Cl} decreases and N_O increases upon treatment in 2.5% H_2 in He at 773 K. On the other hand, the elemental analysis of spent Zn/H-MFI (Zn/Al = 0.23) has shown that nearly all Cl has been removed from this sample (Cl/Zn = 0.07; see Table 2). This discrepancy may exist because, to achieve a high signal-to-noise ratio, significantly more Zn/H-MFI was used for XAFS measurements than for kinetic studies. Furthermore, Zn/H-MFI was packed as a dense pellet for XAFS measurements. Taken together, these factors may have impeded the rate at which Cl was removed from Zn/H-MFI during XAFS experiments. Therefore, it is likely that the EXAFS spectra of Zn/H-MFI under 2.5% H_2 in He at 773 K do not accurately reflect the state of the catalyst after treatment in 2.5% H_2 in He for 7 h prior to reaction rate measurements and during C_3H_8 dehydrogenation in the presence of cofed H_2. In actuality, Zn/H-MFI catalysts of lower Zn loadings (i.e., not containing $ZnAl_2O_4$/$ZnAl_2O_{4-x}Cl_{2x}$ nanoclusters) contain negligible Cl.

The EXAFS fitting results suggest that the as-prepared Zn/H-MFI catalysts of all Zn loadings contain predominantly $[ZnCl]^+$ cations coordinated to two framework O atoms. The formation of $[ZnCl]^+$ cations in $ZnCl_2$-modified zeolites has been proposed previously.[16−18,47,61] The $[ZnCl]^+$ cations may exist preferentially as $[ZnCl]^+$−$[ZnCl]^+$ pairs located at cation-exchange sites associated with pairs of proximate Al atoms. Electrostatic repulsion or steric hindrance between proximate $[ZnCl]^+$ cations may prevent the Zn centers from coordinating to three O atoms in the zeolite framework. Treatment in 2.5% H_2 in He results in the partial conversion of $[ZnCl]^+$ cations. It is possible that $[ZnCl]^+$ cations are converted to $[ZnH]^+$

https://doi.org/10.1021/acscatal.1c03641
ACS Catal. 2021, 11, 14489−14506

cations. The conversion of $[ZnCl]^+$ to $[ZnH]^+$ would be accompanied by the release of HCl. Given that ICP-OES also shows Zn loss from spent catalysts, it is possible that upon treatment in 2.5% H_2 in He, a fraction of $[ZnH]^+$ or $[ZnCl]^+$ species reacts with H_2, resulting in the regeneration of a Brønsted acid site and the loss of Zn as gas-phase ZnH_xCl_y. The Zn species may then exist as $[ZnH]^+-H^+$ pairs in which the Zn center is coordinated to three O atoms in the framework; the loss of the adjacent $[ZnCl]^+$ cation plausibly alleviates the electrostatic repulsion or steric hindrance that would otherwise prevent the formation of a third Zn−O bond to the framework. The formation of $[ZnH]^+$ species in Zn-exchanged zeolites during H_2 treatment or light alkane dehydrogenation has been demonstrated experimentally[24,26,29,30,33−35] and theoretically[31,32,66−68] at cation-exchange sites associated with proximate pairs of framework Al atoms,[32,34,35,66,67] distant pairs of framework Al atoms,[24,26,29,33] or isolated framework Al atoms.[31]

In addition to $[ZnCl]^+-[ZnCl]^+$ pairs at proximate Al atoms, $[ZnCl]^+$ cations associated with isolated Al atoms may form once all proximate Brønsted acid sites are exchanged. $[ZnCl]^+$ cations associated with these sites are likely lost as gas-phase ZnH_xCl_y during treatment in 2.5% H_2 in He at 773 K.

We note that the EXAFS results reported here do not support the formation of $[ZnOH]^+$ species coordinated to two framework O atoms upon treatment in 2.5% H_2 in He. Pinilla-Herrero et al. used DFT-assisted EXAFS fitting to establish the presence of $[ZnOH]^+$ cations coordinated to three framework O atoms in Zn/H-MFI prepared by aqueous ion exchange. For $[ZnOH]^+$ cations, they found that the DFT-optimized interatomic distance between Zn and the O atoms of the OH group is shorter than that between Zn and the framework O atoms.[59] Our EXAFS fitting results show that there is no change in R_O upon treatment with 2.5% H_2 in He, and thus it is unlikely that Zn/H-MFI treated in 2.5% H_2 in He contains $[ZnOH]^+$ cations as a significant fraction of all Zn species.

In summary, the characterization of Zn/H-MFI reveals that the Zn speciation is a function of Zn loading and that the structure of Zn sites changes upon postsynthetic treatment. FTIR and ^{1}H MAS NMR show that during SSIE, Zn species interact primarily with Brønsted acid sites, as opposed to Si−OH groups. The high Cl/Zn ratio and EXAFS analysis of as-prepared Zn/H-MFI catalysts suggest that they contain predominantly three-coordinate $[ZnCl]^+$ and $[ZnCl(HCl)]^+$ species. For Zn/H-MFI with Zn/Al ratios of 0.06−0.52, FTIR spectra of adsorbed pyridine suggest that only isolated Lewis acidic Zn sites are formed; however, at higher Zn loadings, nanoclusters of $ZnAl_2O_4$ or $ZnAl_2O_{4-x}Cl_{2x}$ may be present, as evidenced by ^{27}Al MAS NMR and UV−vis DRS. As shown in Scheme 1, the treatment of as-prepared Zn/H-MFI catalysts in He at 773 K results in the desorption of adsorbed HCl and hence the conversion of $[ZnCl(HCl)]^+$ species to $[ZnCl]^+$ cations. Upon further treatment in 2.5% H_2 in He at 773 K, $[ZnCl]^+$ cations may be converted to $[ZnH]^+$ cations. However, our kinetic data (discussed below) suggest that during C_3H_8 dehydrogenation in the absence of cofed H_2, the $[ZnH]^+$ cations that may form might be converted to bridging Zn^{2+} cations. Our data also suggest that this transformation is reversible; $[ZnH]^+$ cations may be regenerated when H_2 is introduced to the C_3H_8 feed.

It should be noted that we were not able to directly detect the formation of $[ZnH]^+$ cations via in situ FTIR experiments

Scheme 1. Proposed Zn Speciation in Zn/H-MFI after Solid-State Ion Exchange of $ZnCl_2$ and Removal of Cl[a]

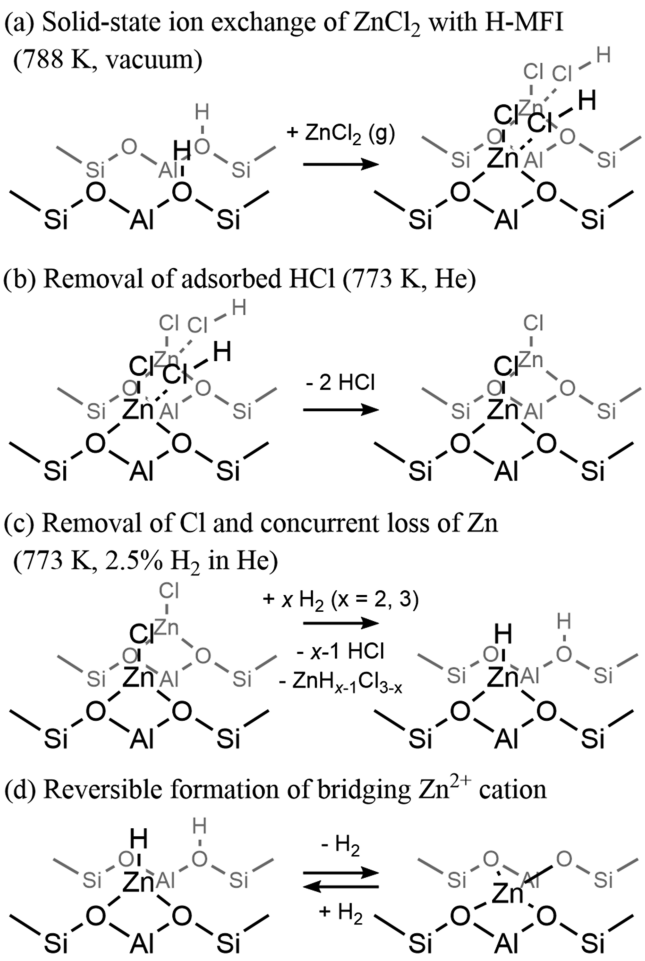

[a](a) Solid-state ion exchange of $ZnCl_2$ with Brønsted acid protons in H-MFI is carried out at 788 K under vacuum, resulting in the formation of $[ZnCl]^+$ and $[ZnCl(HCl)]^+$ species. The formation of $ZnAl_2O_4/ZnAl_2O_{4-x}Cl_{2x}$ nanoclusters occurs as well at high catalyst Zn/Al loadings but is not depicted here. (b) HCl desorbs from the as-prepared Zn/H-MFI upon heating in He at 773 K. (c) Loss of Cl and Zn occurs upon further treatment in 2.5% H_2 in He at 773 K. This may result in the formation of $[ZnH]^+$ cations. (d) As discussed below, when H_2 is not present in the feed, the $[ZnH]^+$ cations that may form might be converted to bridging Zn^{2+} cations; this transformation is reversible.

performed under 2.5% H_2/He at 473−773 K. FTIR has been previously used to observe the formation of $[ZnH]^+$ cations in Zn/H-MFI in the presence of H_2. Specifically, it has been observed that $[ZnH]^+$ cations form upon dissociative adsorption of H_2 over Zn^{2+} cations stabilized at pairs of distant Al atoms in high-silica zeolites.[24,26,29,33] Additionally, $[ZnH]^+$ cations form upon the dissociative adsorption of H_2 over Zn^{2+} sites located at circumferentially oriented pairs of proximate Al atoms within the MFI straight channels.[32,34,35] However, our kinetic data (discussed below) suggests that the $[ZnH]^+$ cations we propose in this work may differ with respect to their location in the MFI channel system and/or the distribution of the Al atoms for which they charge-compensate. It is thus not clear whether $[ZnH]^+$ cations are formed in the Zn/H-MFI catalysts prepared in this work. However, recent theoretical work has shown that $[ZnH]^+$ cations may form

https://doi.org/10.1021/acscatal.1c03641
ACS Catal. 2021, 11, 14489−14506

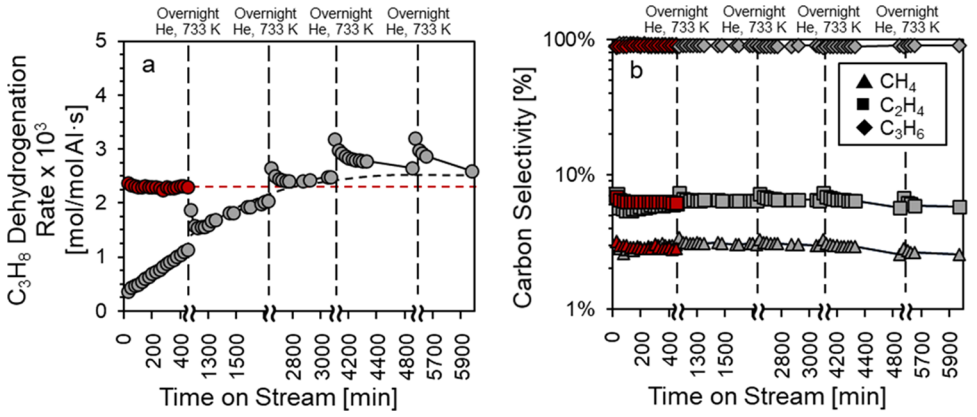

Figure 8. (a) Rate of C_3H_8 dehydrogenation over Zn/H-MFI (Zn/Al = 0.94 in the as-prepared sample and 0.36 in the spent sample) and (b) product distribution at 733 K, 0.9 kPa C_3H_8, and a space time τ = 9 mol Al·s/mol C_3H_8. Gray data points indicate Zn/H-MFI not treated in H_2. Red data points indicate Zn/H-MFI treated in 2.5% H_2 in He at 773 K for 7 h.

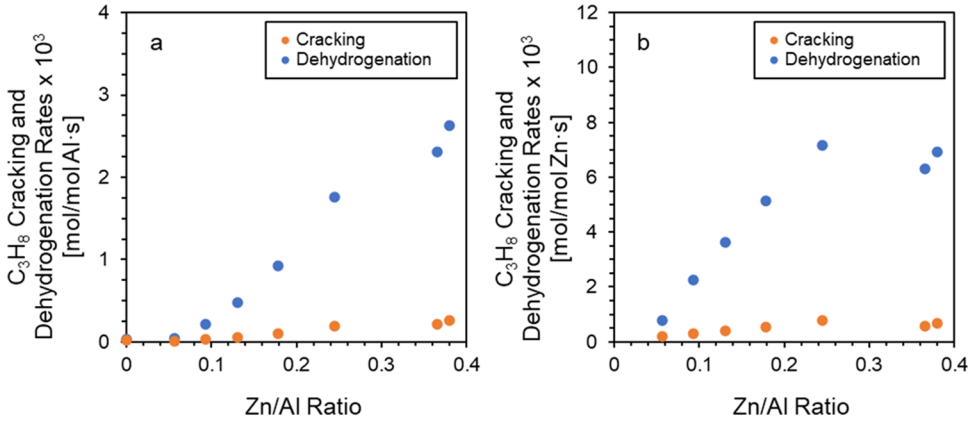

Figure 9. Effect of Zn loading (in spent catalyst samples) on rates of C_3H_8 dehydrogenation and cracking (extrapolated to zero space time) over Zn/H-MFI normalized (a) per Al atom and (b) per Zn atom in spent samples (Zn/Al = 0.06−0.36) at 733 K, 1 kPa C_3H_8.

within the MFI channel intersections but they are less stable relative to $[ZnOH]^+$ cations or Zn^{2+} cations.[31] Therefore, it is possible that even if $[ZnH]^+$ cations are formed in our Zn/H-MFI samples in the presence of 2.5% H_2/He, they may be present in a sufficiently low concentration such that they cannot be detected by FTIR.

3.2. C_3H_8 Conversion over H-MFI. The kinetics of C_3H_8 conversion over H-MFI were measured; CH_4, C_2H_4, and C_3H_6 are formed via monomolecular dehydrogenation and cracking. The rate of C_3H_8 dehydrogenation over H-MFI initially decreased with time on stream for the first 3 h of reaction. During that time, the rate of C_3H_8 cracking remained approximately constant. These observations are qualitatively consistent with trends previously reported for C_3H_8 and *n*-C_4H_{10} dehydrogenation and cracking over H-MFI. The initially higher C_3H_8 dehydrogenation activity of H-MFI has been attributed to Lewis acidic extraframework Al (EFAL) sites that deactivate with increasing time on stream.[5,69] Rate measurements reported here were performed at steady state after the initial deactivation period. Reaction rates and product carbon selectivities were extrapolated to zero space time. For all reaction conditions employed, the ratio of the carbon selectivity of C_2H_4 to that of CH_4 extrapolates to ∼2 at zero space time. This corresponds to a molar ratio of C_2H_4 to CH_4 of ∼1. This is consistent with the formation of CH_4 and C_2H_4 as primary products of monomolecular C_3H_8 cracking.

C_3H_8 dehydrogenation and cracking rates were measured as a function of temperature (753−773 K) for a C_3H_8 partial pressure of 1 kPa. Arrhenius plots are shown in Figure S12. The apparent activation energy for C_3H_8 cracking is 34.2 ± 2.2 kcal/mol and that for C_3H_8 dehydrogenation is 38.1 ± 0.04 kcal/mol. The measured apparent activation energies are consistent with those previously reported for C_3H_8 cracking (35.1−40.6 kcal/mol) and dehydrogenation (22.7−47.8 kcal/mol) over H-MFI.[5,70−73]

3.3. C_3H_8 Conversion over Zn/H-MFI. The rate of C_3H_8 dehydrogenation over as-prepared Zn/H-MFI (Zn/Al = 0.94) as a function of time on stream is shown in Figure 8a, and the product distribution is shown in Figure 8b. The rate of C_3H_8 dehydrogenation over Zn/H-MFI increases with time on stream over the course of several days, although the product distribution remains unchanged. These trends suggest that a single type of Zn site contributes to the observed rate and that the concentration of this site grows with time on stream.

When as-prepared Zn/H-MFI is treated in 2.5% H_2 in He for 7 h at 773 K and then held overnight in He prior to measurement of the rate of C_3H_8 dehydrogenation, no induction period is observed. This suggests that reaction with H_2 is responsible for the transformation of $[ZnCl]^+$ cations in the as-prepared catalyst to their active forms. Our EXAFS analysis and elemental analysis suggest that the reaction of H_2 with $[ZnCl]^+$ cations results in the removal of the Cl ligand. We also observe that once the catalyst reaches its

https://doi.org/10.1021/acscatal.1c03641
ACS Catal. 2021, 11, 14489−14506

steady-state activity, it is stable with regard to activity and selectivity for nearly 100 h of use.

3.4. Effect of Zn Loading on C_3H_8 Conversion over Zn/H-MFI. The effect of Zn loading on the product distribution and kinetics of C_3H_8 dehydrogenation and cracking was investigated over Zn/H-MFI (Zn/Al = 0.06−0.38 in spent catalysts). The trends are identical for all temperatures (713−773 K) and C_3H_8 partial pressures (0.8−4.5 kPa). Figure 9a shows the C_3H_8 dehydrogenation and cracking rates normalized per Al atom, measured at 733 K and 1 kPa C_3H_8, as a function of Zn loading in spent catalysts. The dehydrogenation and cracking rates normalized per Al atom increase with increasing Zn loading. For example, rates of dehydrogenation and cracking over Zn/H-MFI (Zn/Al = 0.24) are ∼53× and ∼8× higher, respectively, compared to those of H-MFI at identical reaction conditions, whereas dehydrogenation and cracking rates over Zn/H-MFI (Zn/Al = 0.09) are only ∼6× and ∼1.1× higher, respectively. The product distribution (extrapolated to zero space time) is shown in Figure 10. For Zn/H-MFI (Zn/Al = 0.06), the carbon

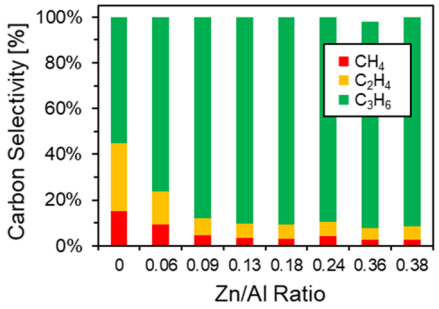

Figure 10. Effect of Zn loading (in spent catalyst samples) on the product distribution (extrapolated to zero space time) of C_3H_8 conversion over Zn/H-MFI (Zn/Al = 0.06−0.36 in spent samples) at 733 K, 1 kPa C_3H_8.

selectivity to C_3H_6 is 76%. This corresponds to a ratio of C_3H_8 dehydrogenation-to-cracking rates of 4.1. As the Zn loading is increased to Zn/Al = 0.13, the carbon selectivity to C_3H_6 increases to 90%, corresponding to a ratio of dehydrogenation-to-cracking rates of 8.5. The lower selectivity to C_3H_6 observed for C_3H_8 conversion over Zn/H-MFI (Zn/Al = 0.6−0.09) is likely due to C_3H_8 conversion over residual Brønsted acid sites in addition to Zn sites. As the Zn loading is further increased to Zn/Al = 0.38, little change in the product distribution is observed. This is consistent with the presence of a single active Zn site across all Zn/H-MFI samples.

The C_3H_8 dehydrogenation and cracking rates normalized per Zn atom in spent catalysts are shown as a function of Zn loading in spent catalysts in Figure 9b. The dehydrogenation and cracking rates normalized per Zn atom in the spent catalyst increase with increasing Zn loading for Zn/Al = 0.06−0.24. We have noted above that these catalysts contain only isolated Zn sites and that a single type of active Zn site exists. As 40% of all Al atoms in the MFI zeolite used in this work are present as next-nearest neighbors (NNNs) or next-next-nearest neighbors (NNNNs),[69] the maximum Zn/Al ratio achievable if all Zn atoms were present as bridging Zn^{2+} cations is ∼0.20. This estimate is similar to the Zn content of spent Zn/H-MFI corresponding to the maximum activity (per Zn atom), indicating that in the absence of cofed H_2, Zn sites are likely associated with pairs of proximate framework Al atoms as bridging Zn^{2+} cations. The catalytic activity of Zn^{2+} cations for light alkane dehydrogenation and aromatization has recently received considerable attention.[31,74−76] In particular, in situ NMR has been used to demonstrate the promoting effect of Zn^{2+} cations in H-BEA on propane and butane aromatization and C−H bond activation and to investigate the mechanism by which this occurs.[74−76]

No further increase in the dehydrogenation and cracking rates is observed when the Zn/Al ratio is increased beyond Zn/Al = 0.24. This is likely due to the presence of less active $ZnAl_2O_4/ZnAl_2O_{4-x}Cl_{2x}$ nanoclusters in Zn/H-MFI samples with Zn/Al ratios of 0.38 and 0.36 (corresponding to Zn/Al = 0.79 and 0.94 in as-prepared catalysts). These findings parallel previous work demonstrating that $ZnAl_2O_4$ species in Zn-exchanged H-MFI/Al_2O_3 catalysts exhibit low dehydrogenation activity during the conversion of methanol to aromatics.[77]

These results suggest that although a single type of Lewis acidic Zn active site, namely, Zn^{2+} cations, catalyzes C_3H_8 dehydrogenation and cracking over Zn/H-MFI (Zn/Al = 0.06−0.24), there is a systematic variation in the activity of Zn^{2+} cations as a function of Zn/Al ratio; the more active Zn^{2+} cations are formed in greater proportions at higher Zn/Al ratios.

This variation in the catalytic activity of Zn^{2+} cations may be attributed to differences in the siting and distribution of framework Al atoms at their corresponding cation-exchange sites. The siting of Al atoms refers to both their location in individual rings in the zeolite framework and to their position in the zeolite channels and channel intersections.[78] In MFI, three unique Al−O−(Si−O)$_2$−Al sequences situated in one framework ring, each corresponding to a different position in the zeolite channels and channel intersections, have been identified; these positions are denoted the α-, β-, and γ-sites. The α-site is situated in the straight channels of MFI, the β-site is situated at the channel intersections, and the γ-site is situated in the sinusoidal channels.[78] The distribution of Al atoms refers to their arrangement as, for example, Al−O−Si−O−Al sequences, i.e., next-nearest neighbors (NNNs), Al−O−(Si−O)$_2$−Al sequences, i.e., next-next-nearest neighbors (NNNNs), or isolated Al atoms; it is possible to further distinguish between pairs of proximate Al atoms situated in the same or different rings.[78] The effects of Al siting and distribution on the stability and catalytic activity of Zn^{2+} cations have been widely investigated using DFT calculations for a range of zeolite framework topologies. van Santen et al. have reported that Zn^{2+} cations located in the 5-membered rings in straight or sinusoidal channels of MFI are more stable relative to Zn^{2+} cations in the 4-membered rings or at the α-site. The authors note that in general, increasing the stability of a site lowers its catalytic activity; this relationship was demonstrated for the dissociative adsorption of C_2H_6 and H_2 over varying Zn sites.[79] Benco et al. have reported that Zn^{2+} cations in Zn/MOR are more stable at cation-exchange sites associated with proximate Al atoms located in one ring, as opposed to distant Al atoms. Furthermore, the authors found that the adsorption and dissociation of H_2 and CH_4 are more exothermic over less stable Zn^{2+} sites.[80] Likewise, Barbosa et al. have reported that the stability of Zn^{2+} cations in the 8-membered rings (8-MR) of CHA, MOR, and FER is a function of the distance between framework Al atoms; for all framework topologies investigated, Zn^{2+} cations are most stable at cation-exchange sites associated with NNN Al atoms.[68] Mahyuddin et

https://doi.org/10.1021/acscatal.1c03641
ACS Catal. 2021, 11, 14489−14506

al. have reported that the relative stability of Zn^{2+} cations in 6- and 8-MRs of Zn/MFI depends on the Al siting and distribution and that the greater stability of Zn^{2+} cations in 6-MRs relative to 8-MRs leads to a higher energy barrier for methane activation.[65] Similarly, Albarracín-Suazo et al. have found that the siting of Al atoms in the α-ring of Zn/MFI affects the stability of Zn^{2+} cations and that the most stable configuration gives rise to the largest energy barrier for methane activation.[81] Finally, Oda et al. have shown that the arrangement of Al pairs in Zn/MFI (either in the circumferential direction of the straight channel or along its axis) determines the activity of Zn^{2+} cations for the heterolytic cleavage of H_2, which proceeds spontaneously only over the least stable Zn^{2+} site.[32]

The effect of Al siting and distribution has also been investigated for alkane dehydrogenation and cracking over Brønsted acid sites in H-MFI. Janda et al. have noted that n-butane dehydrogenation over H-MFI occurs preferentially at channel intersections due to the lower confinement of the dehydrogenation transition state,[69] whereas Song et al. found that alkane cracking rates are higher at proximate, rather than isolated, Brønsted acid sites due to the more positive intrinsic entropies of activation.[82]

The studies referenced above demonstrate that Al siting and distribution can affect the stability and catalytic activity of extraframework cations in multiple ways. It is expected that the catalytic activity of Zn^{2+} sites in Zn/H-MFI prepared in this work will depend on the Al siting and distribution. As the Al siting in MFI cannot be completely determined,[78,83] and because of the multiple ways in which the Al siting and distribution may affect the catalytic activity, the cause of the observed increase in dehydrogenation and cracking activity with Zn loading cannot be determined based on the data reported here. It is, nevertheless, plausible that Zn^{2+} sites formed at higher Zn loadings are located at cation-exchange sites associated with increasingly distant pairs of Al atoms and that these sites exhibit decreased stability and increased catalytic activity. It is also plausible that Zn^{2+} sites formed at higher Zn loadings are preferentially situated at the β-site in MFI and the increased dehydrogenation and cracking activity are due to more positive intrinsic entropies of activation.

Apparent activation energies ($E_{a,app}$) for C_3H_8 dehydrogenation and cracking were measured as a function of Zn loading and are given in Table 5, along with the corresponding data for H-MFI. The apparent activation energies for dehydrogenation and cracking are similar to each other for all Zn loadings and consistent with the apparent activation energies reported previously (29.8 and 31.2 kcal/mol for C_3H_8 dehydrogenation and cracking, respectively).[84] The apparent activation energies for C_3H_8 dehydrogenation and cracking generally appear to increase slightly as the Zn/Al ratio of spent catalysts increases from 0.06 to 0.24. The apparent entropies of activation for C_3H_8 dehydrogenation and cracking also generally appear to increase slightly with increasing catalyst Zn loading, as shown in Figure S14.

3.5. Effect of Cofeeding H_2 on C_3H_8 Conversion over Zn/H-MFI. The effect of cofeeding H_2 during C_3H_8 conversion over Zn/H-MFI (Zn/Al = 0.13 in the spent catalyst) was investigated. Table 6 shows that upon introduction of 0.5 kPa H_2 to a feed of 0.8 kPa C_3H_8, the rate of C_3H_8 dehydrogenation decreases and the rate of C_3H_8 cracking increases. The decreased rate of C_3H_8 dehydrogenation is not consistent with the competitive adsorption of H_2 and C_3H_8 on the active site that catalyzes both dehydrogenation and cracking. Furthermore, the catalyst activity was restored by treating the catalyst overnight in He at 733 K, indicating that the decrease in activity upon exposure to H_2 was not due to reduction of Zn species or loss of Zn species from the catalyst bed. Additionally, no C_2H_6 was formed as a result of cofeeding H_2, indicating that the increased rate of C_3H_8 cracking is not due to hydrogenolysis of C_3H_8. This finding differs from recent in situ NMR studies showing that Zn^{2+} cations in Zn/H-BEA catalyze C_3H_8 hydrogenolysis.[75] Finally, the decrease in the rate of C_3H_8 dehydrogenation is not due to an approach to equilibrium; the C_3H_8 conversion of <2% is significantly lower than the equilibrium conversions of 76 and 65% for this reaction in the absence and presence of cofed H_2, respectively. Taken together, these observations suggest that the decreased C_3H_8 dehydrogenation rate over Zn/H-MFI is due to the transformation of the active zinc species in the presence of H_2.

Table 5. Apparent Activation Energies for C_3H_8 Dehydrogenation and Cracking over H-MFI and Zn/H-MFI[a]

zeolite	Zn/Al (as-prepared)	Zn/Al (spent)	apparent activation energy [kcal/mol]	
			cracking	dehydrogenation
H-MFI			34.2 ± 2.2	38.1 ± 0.04
Zn/H-MFI	0.06	0.06	23.9 ± 6.6	25.5 ± 3.6
	0.15	0.09	28.6 ± 4.4	32.8 ± 1.1
	0.23	0.13	28.9 ± 3.5	31.6 ± 1.4
	0.34	0.18	31.9 ± 2.4	33.0 ± 1.5
	0.52	0.24	31.4 ± 1.6	30.8 ± 0.5
	0.79	0.38	31.6 ± 3.1	29.3 ± 2.0
	0.94	0.36	27.8 ± 5.3	27.1 ± 2.2

[a]Reaction conditions: 713−773 K, 1 kPa C_3H_8. All rates were extrapolated to zero space time. Error bars indicate 95% confidence intervals.

We proposed that upon treatment of as-prepared Zn/H-MFI in 2.5% H_2 in He at 773 K, $[ZnH]^+$ cations may be formed. We also proposed that in the absence of cofed H_2, Zn^{2+} cations catalyze C_3H_8 dehydrogenation and cracking. $[ZnH]^+$ cations may be converted to Zn^{2+} cations via reaction with a nearby Brønsted acid proton; this would be accompanied by the release of H_2. The Zn^{2+} cations exhibit higher dehydrogenation activity and lower cracking activity compared to $[ZnH]^+$ cations, as shown in Table 5. This result agrees with DFT calculations recently reported by Du et al.[31]

3.6. Effect of C_3H_8 Partial Pressure and Temperature on C_3H_8 Conversion over Zn/H-MFI. The effects of temperature and C_3H_8 partial pressure on the product distribution and kinetics of C_3H_8 dehydrogenation and cracking were investigated over Zn/H-MFI (Zn/Al = 0.06−0.38 in spent catalysts). The trends are identical for catalysts of all Zn loadings. Figure 11 shows the rates of C_3H_8 dehydrogenation and cracking over Zn/H-MFI (Zn/Al = 0.13) as a function of C_3H_8 partial pressure and temperature. The C_3H_8 dehydrogenation and cracking rates are normalized per mol Zn in the spent catalyst. At lower C_3H_8 partial pressures and higher temperatures, the dehydrogenation and cracking rates increase with increasing C_3H_8 partial pressure. At higher C_3H_8 partial pressures and lower temperatures, the dehydrogenation and cracking rates approach zero-order kinetics. The product distribution (extrapolated to zero space

https://doi.org/10.1021/acscatal.1c03641
ACS Catal. 2021, 11, 14489−14506

Table 6. Cofeeding H_2 during C_3H_8 Dehydrogenation and Cracking over Zn/H-MFI (Zn/Al = 0.23 in the As-Prepared Sample)[a]

			carbon selectivity [%]		
H_2 partial pressure [kPa]	C_3H_8 dehydrogenation rate [mol C_3H_8/mol Al·s]	C_3H_8 cracking rate [mol C_3H_8/mol Al·s]	CH_4	C_2H_4	C_3H_6
0	5.6×10^{-4}	7.2×10^{-5}	4	8	88
0.5	4.5×10^{-4}	1.1×10^{-4}	6	14	80

[a]Reaction conditions: 753 K, 0.8 kPa C_3H_8, space time 18 mol Al·s/mol C_3H_8. Conversion: <2%.

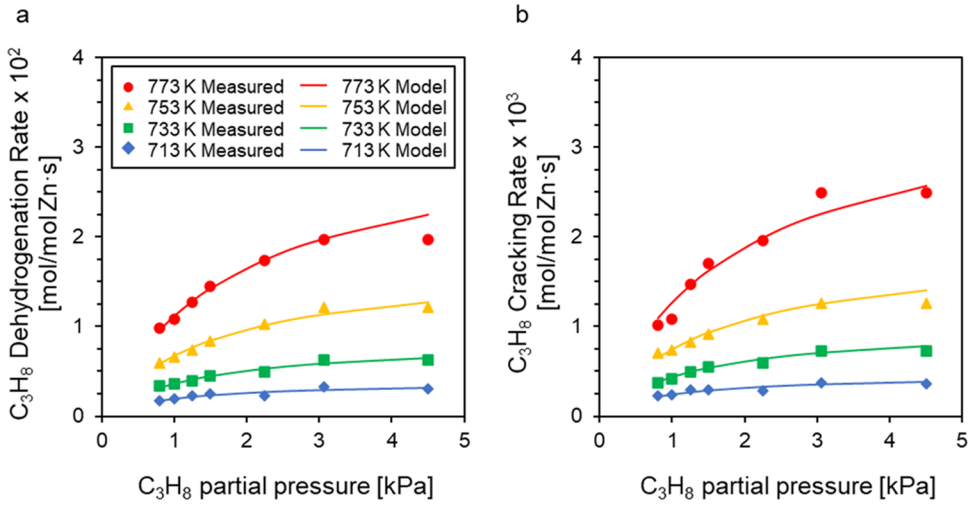

Figure 11. Effect of C_3H_8 partial pressure and temperature on the rates of (a) C_3H_8 dehydrogenation and (b) C_3H_8 cracking (extrapolated to zero space time) over Zn/H-MFI (Zn/Al = 0.13 in the spent sample). The dehydrogenation and cracking rates are normalized per Zn atom in the spent sample.

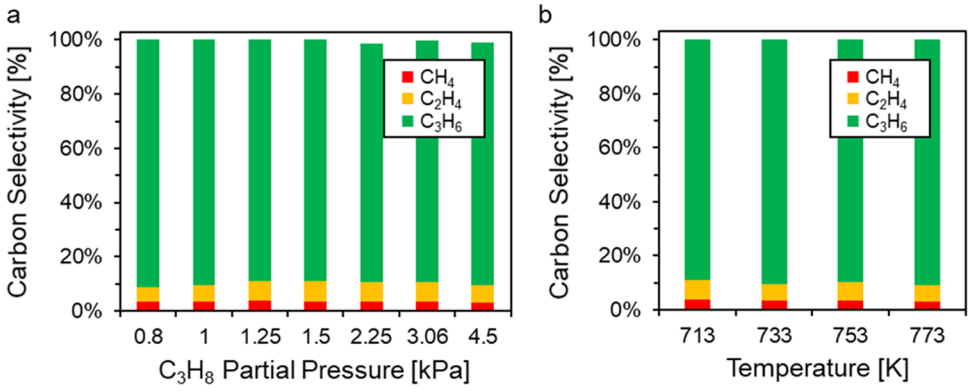

Figure 12. Effect of (a) C_3H_8 partial pressure and (b) temperature on the product distribution (extrapolated to zero space time) of C_3H_8 conversion over Zn/H-MFI (Zn/Al = 0.13 in the spent sample).

time) is shown as a function of the C_3H_8 partial pressure in Figure 12a and as a function of temperature in Figure 12b. No trends in the product distribution, or equivalently the ratio of the rates of C_3H_8 dehydrogenation to cracking, were observed as a function of the C_3H_8 partial pressure. This suggests that the C_3H_8 dehydrogenation and cracking pathways proceed through a common surface intermediate over Zn sites. Furthermore, no trends in the product distribution were observed as a function of temperature. This indicates that the C_3H_8 dehydrogenation and cracking pathways have similar apparent activation energies, as shown in Section 3.4. The product distribution is therefore determined solely by the difference in the entropy of activation for the dehydrogenation vs cracking transition states.

The observed rates of C_3H_8 dehydrogenation and cracking can be described by rate laws of the form given by eqs 1 and 2

$$r_{\text{Dehydrogenation}} = \frac{k_{\text{int,D}} K_{C_3H_8} P_{C_3H_8}}{1 + K_{C_3H_8} P_{C_3H_8}} \quad (1)$$

$$r_{\text{Cracking}} = \frac{k_{\text{int,C}} K_{C_3H_8} P_{C_3H_8}}{1 + K_{C_3H_8} P_{C_3H_8}} \quad (2)$$

In eqs 1 and 2, the rates of dehydrogenation and cracking have units of mol/mol Zn·s. The intrinsic rate coefficients for C_3H_8 dehydrogenation and cracking are denoted by $k_{\text{int,D}}$ and $k_{\text{int,C}}$, respectively, which have units of mol/mol Zn·s. The equilibrium constant for C_3H_8 adsorption is denoted by $K_{C_3H_8}$, which has units of kPa^{-1}. The values of the kinetic

https://doi.org/10.1021/acscatal.1c03641
ACS Catal. 2021, 11, 14489−14506

Table 7. Kinetic and Thermodynamic Parameters for C_3H_8 Dehydrogenation and Cracking over Zn/H-MFI (Zn/Al = 0.13 in the Spent Sample)[a] and Ga/H-MFI (Ga/Al = 0.2)[b] at 733 K[c]

zeolite	$k_{int,D}$ [mol/mol Zn·s or mol/mol Ga·s]	$k_{int,C}$ [mol/mol Zn·s or mol/mol Ga·s]	$K_{C_3H_8}$ [kPa^{-1}]	$k_{app,D}$ ($k_{int,D}K_{C_3H_8}$) [mol/mol Zn·s·kPa or mol/mol Ga·s·kPa]	$k_{app,C}$ ($k_{int,C}K_{C_3H_8}$) [mol/mol Zn·s·kPa or mol/mol Ga·s·kPa]
Zn/H-MFI	8.3×10^{-3}	1.0×10^{-3}	7.8×10^{-1}	6.5×10^{-3}	7.8×10^{-4}
Ga/H-MFI	6.5×10^{-2}	3.2×10^{-3}	2.8	1.8×10^{-1}	9.0×10^{-3}

[a]Obtained via nonlinear least-squares regression analysis of rate data measured at 733 K shown in Figure 11 to eqs 1 and 2. [b]Rate coefficients for dehydrogenation and cracking [with units of mol/mol Al·s] and the equilibrium constant for C_3H_8 adsorption were reported in ref 5. Rate coefficients reported in this table [with units of mol/mol Ga·s] were calculated based on those reported in ref 5. [c]Reported uncertainties reflect 95% confidence intervals.

Table 8. Intrinsic Enthalpies and Entropies of Activation and Enthalpy and Entropy of Adsorption for C_3H_8 Dehydrogenation and Cracking over Zn/H-MFI (Zn/Al = 0.13 in the Spent Sample)[a] and Ga/H-MFI (Ga/Al = 0.2)[b]

	Zn/H-MFI		Ga/H-MFI	
kinetic parameter	$\Delta H^{\ddagger}_{int}$ or ΔH_{ads} [kcal/mol]	$\Delta S^{\ddagger}_{int}$ or ΔS_{ads} [cal/mol·K]	$\Delta H^{\ddagger}_{int}$ or ΔH_{ads}[c] [kcal/mol]	$\Delta S^{\ddagger}_{int}$ or ΔS_{ads}[d] [cal/mol·K]
$k_{int,C}$	35.8 ± 1.7	−25.3 ± 2.3	42.0 ± 4.7	−14.4 ± 6.4
$K_{C_3H_8}$	−12.1 ± 2.2	−7.7 ± 3.0	−15.6 ± 5.0	−19.2 ± 6.8
$k_{int,D}$	37.3 ± 1.5	−19.0 ± 2.0	34.6 ± 1.0	−18.5 ± 1.4

[a]Obtained via linear least-squares regression analysis of data shown in Figure S16 to eqs S3, S4, and S7. [b]Reported uncertainties reflect 95% confidence intervals. [c]Reported in ref 5. [d]Calculated from rate coefficients for dehydrogenation and cracking [with units of mol/mol Ga·s] shown in Table 7 and from $\Delta H^{\ddagger}_{int}$ and ΔH_{ads} reported in ref 5.

parameters $k_{int,C}$, $k_{int,D}$, and $K_{C_3H_8}$ at 713−773 K were obtained by fitting eqs 1 and 2 to the measured rates of C_3H_8 dehydrogenation and cracking at each temperature; the fits are represented by the solid lines in Figure 11. Parity plots are shown in Figure S15, and the fitted values of the kinetic parameters at 733 K are reported in Table 7. Also reported in Table 7 are the apparent first-order rate coefficients for C_3H_8 dehydrogenation and cracking, denoted by $k_{app,D}$ and $k_{app,C}$, respectively. Intrinsic enthalpies ($\Delta H^{\ddagger}_{int}$) and entropies ($\Delta S^{\ddagger}_{int}$) of activation for C_3H_8 cracking and dehydrogenation, and the enthalpy (ΔH_{ads}) and entropy (ΔS_{ads}) of adsorption of C_3H_8, were obtained by fitting eqs S3, S4, and S7 to the data in Figure S16; the results are reported in Table 8. The entropy of activation for C_3H_8 dehydrogenation is less negative than that for cracking, and the enthalpies of activation are similar to each other. These results are expected based on the higher rate of C_3H_8 dehydrogenation relative to cracking over Zn/H-MFI and the absence of an effect of temperature on the selectivity to dehydrogenation over cracking.

The kinetics and thermodynamics of C_3H_8 dehydrogenation and cracking over Zn/H-MFI can be compared to those for Ga/H-MFI prepared by SSIE of $GaCl_3$ with the same parent H-MFI zeolite used in this study.[5] The rates of C_3H_8 dehydrogenation and cracking over Ga/H-MFI prepared via SSIE of $GaCl_3$ decrease with increasing Ga content because $[GaH]^{2+}$ cations, which are formed upon treatment in H_2 and are the most active Ga species for C_3H_8 conversion, exist in greater proportions at low Ga/Al ratios.[5,6] By contrast, Zn^{2+} cations formed in Zn/H-MFI at higher Zn/Al ratios are more active for C_3H_8 dehydrogenation and cracking. The intrinsic rate coefficients for C_3H_8 dehydrogenation and cracking over Ga/H-MFI (Ga/Al = 0.2) were reported in ref 5 and are shown in Table 7. The intrinsic rate coefficient for C_3H_8 dehydrogenation at 733 K is nearly an order of magnitude higher for Ga/H-MFI compared to that for Zn/H-MFI, although there is no difference in the intrinsic enthalpies of activation for C_3H_8 dehydrogenation. The intrinsic rate coefficient for cracking at 733 K is ∼3× higher for Ga/H-MFI relative to Zn/H-MFI, although the intrinsic enthalpy of activation for C_3H_8 cracking is higher. Additionally, the equilibrium constant for C_3H_8 adsorption is ∼3.5× higher for Ga/H-MFI relative to Zn/H-MFI at 733 K, at least in part due to stronger adsorption of C_3H_8 on Ga/H-MFI. The apparent first-order rate coefficients for dehydrogenation and cracking are thus ∼28× and ∼12× higher, respectively, over Ga/H-MFI compared to Zn/H-MFI at 733 K, and therefore, the ratio of dehydrogenation-to-cracking rates is greater (∼20 at 733 K) for reaction over Ga/H-MFI compared to that over Zn/H-MFI (∼8.4 at 733 K), as shown in Table 9.

Table 9. Dehydrogenation-to-Cracking Rate Ratios over Zn/H-MFI (Zn/Al = 0.13 in the Spent Sample) and Ga/H-MFI (Ga/Al = 0.2) at 713−773 K[a]

	dehydrogenation-to-cracking rate ratio	
temperature (K)	Zn/H-MFI	Ga/H-MFI
713	8.2	23.6
718	8.3	22.6
733	8.4	20.3
753	8.7	17.7
773	8.9	15.6

[a]Calculated from $\Delta H^{\ddagger}_{int}$ and $\Delta S^{\ddagger}_{int}$ for C_3H_8 dehydrogenation and cracking shown in Table 8.

4. CONCLUSIONS

Zn/H-MFI was prepared via solid-state ion exchange of $ZnCl_2$ to achieve different zeolite Zn/Al ratios. For Zn/H-MFI catalysts with as-prepared Zn/Al ratios between 0.06 and 0.52, Zn is present primarily as Lewis acidic $[ZnCl]^+$ and $[ZnCl(HCl)]^+$ cations. At higher Zn loadings, there is some evidence for $ZnAl_2O_4$ and/or $ZnAl_2O_{4-x}Cl_{2x}$ nanoclusters. Treatment of as-prepared Zn/H-MFI in He at 773 K results in the desorption of HCl, that is, conversion of $[ZnCl(HCl)]^+$ to $[ZnCl]^+$ cations. Further treatment in 2.5% H_2 in He for 7 h at 773 K prior to reaction may result in the conversion of $[ZnCl]^+$ to $[ZnH]^+$ cations. Kinetic data suggests that during C_3H_8 dehydrogenation, $[ZnH]^+$ cations are converted to Zn^{2+}

https://doi.org/10.1021/acscatal.1c03641
ACS Catal. 2021, 11, 14489−14506

cations; this is evidenced by the fact that the catalyst Zn/Al ratio corresponding to the highest activity per Zn atom is similar to the maximum Zn/Al ratio achievable if all Zn sites were present as Zn^{2+} cations. The transformation of $[ZnH]^+$ cations to Zn^{2+} cations is reversible; $[ZnH]^+$ cations may be regenerated when H_2 is introduced to the C_3H_8 feed.

The product distribution and kinetics of C_3H_8 dehydrogenation and cracking were measured as a function of C_3H_8 partial pressure, temperature, and Zn loading. C_3H_8 dehydrogenation and cracking are catalyzed by Zn^{2+} cations. The activity of such Zn^{2+} cations increases with the Zn loading due to the localization of Zn^{2+} cations either at increasingly distant pairs of Al atoms or at the β-site in the MFI framework. The selectivity to dehydrogenation over cracking is independent of the C_3H_8 partial pressure and temperature, indicating that the dehydrogenation and cracking pathways proceed via a common surface intermediate and have similar enthalpies of activation and that the selectivity to dehydrogenation over cracking is governed by the difference in the entropy of activation associated with each pathway. Additionally, we have shown that $[ZnH]^+$ cations that may form in the presence of H_2 exhibit lower dehydrogenation activity and higher cracking activity compared to Zn^{2+} cations. This finding agrees with the recent theoretical work for C_4H_{10} dehydrogenation over Zn/H-MFI.[31]

■ ASSOCIATED CONTENT

Supporting Information

The Supporting Information is available free of charge at https://pubs.acs.org/doi/10.1021/acscatal.1c03641.

Additional data related to catalyst characterization via XRD, FTIR, $^1H-^{27}Al$ TRAPDOR NMR, UV−vis DRS, and XAS; supplementary kinetic data; and additional information pertaining to fitted kinetic and thermodynamic parameters (PDF)

■ AUTHOR INFORMATION

Corresponding Author

Alexis T. Bell − *Department of Chemical and Biomolecular Engineering, University of California, Berkeley, California 94720, United States;* orcid.org/0000-0002-5738-4645; Email: alexbell@berkeley.edu

Authors

Danna Nozik − *Department of Chemical and Biomolecular Engineering, University of California, Berkeley, California 94720, United States*

Francesca Mikaela P. Tinga − *Department of Chemical and Biomolecular Engineering, University of California, Berkeley, California 94720, United States*

Complete contact information is available at: https://pubs.acs.org/10.1021/acscatal.1c03641

Notes

The authors declare no competing financial interest.

■ ACKNOWLEDGMENTS

This work was supported by a grant from Chevron Energy Technology Co. The authors thank Dr. Neelay Phadke, Dr. Liang Qi, and Dr. Yanfei Zhang for helpful technical discussions, Natalie Lefton for help with catalyst preparation, and Dr. Wei-Chih Liao and Dr. Alicia Lund for help with NMR measurements. The authors also gratefully acknowledge Dr. Mark Warren and Dr. Yujia Ding (Illinois Institute of Technology) for help with XAFS measurements. This research used resources of the Advanced Photon Source, a U.S. Department of Energy (DOE) Office of Science User Facility operated for the DOE Office of Science by Argonne National Laboratory under Contract No. DE-AC02-06CH11357. MRCAT operations are supported by the Department of Energy and the MRCAT member institutions. This research also used the resources of the U.C. Berkeley Small Molecule X-ray Crystallography Facility (NIH Shared Instrumentation Grant S10-RR027172).

■ REFERENCES

(1) Xiang, Y.; Wang, H.; Cheng, J.; Matsubu, J. Progress and Prospects in Catalytic Ethane Aromatization. *Catal. Sci. Technol.* **2018**, *8*, 1500−1516.

(2) Saito, H.; Sekine, Y. Catalytic Conversion of Ethane to Valuable Products through Non-Oxidative Dehydrogenation and Dehydroaromatization. *RSC Adv.* **2020**, *10*, 21427−21453.

(3) O'Connor, C. T. Aromatization of Light Alkanes. In *Handbook of Heterogeneous Catalysis*; Ertl, G.; Knözinger, H.; Schüth, F.; Weitkamp, J., Eds.; Wiley-VCH: Weinheim, 2008; pp 3123−3133.

(4) Sweeney, W. A.; Bryan, P. F. BTX Processing. In *Kirk-Othmer Encyclopedia of Chemical Technology*; John Wiley & Sons, Inc.: 2000; pp 1−14.

(5) Phadke, N. M.; Mansoor, E.; Bondil, M.; Head-Gordon, M.; Bell, A. T. Mechanism and Kinetics of Propane Dehydrogenation and Cracking over Ga/H-MFI Prepared via Vapor-Phase Exchange of H-MFI with $GaCl_3$. *J. Am. Chem. Soc.* **2019**, *141*, 1614−1627.

(6) Phadke, N. M.; Van Der Mynsbrugge, J.; Mansoor, E.; Getsoian, A. B.; Head-Gordon, M.; Bell, A. T. Characterization of Isolated Ga^{3+} Cations in Ga/H-MFI Prepared by Vapor-Phase Exchange of H-MFI Zeolite with $GaCl_3$. *ACS Catal.* **2018**, *8*, 6106−6126.

(7) Phadke, N. M.; Mansoor, E.; Head-Gordon, M.; Bell, A. T. Mechanism and Kinetics of Light Alkane Dehydrogenation and Cracking over Isolated Ga Species in Ga/H-MFI. *ACS Catal.* **2021**, *11*, 2062−2075.

(8) Caeiro, G.; Carvalho, R. H.; Wang, X.; Lemos, M. A. N. D. A.; Lemos, F.; Guisnet, M.; Ramôa Ribeiro, F. Activation of C_2-C_4 Alkanes Over Acid and Bifunctional Zeolite Catalysts. *J. Mol. Catal. A: Chem.* **2006**, *255*, 131−158.

(9) Biscardi, J. A.; Meitzner, G. D.; Iglesia, E. Structure and Density of Active Zn Species in Zn/H-ZSM5 Propane Aromatization Catalysts. *J. Catal.* **1998**, *179*, 192−202.

(10) Biscardi, J. A.; Iglesia, E. Structure and Function of Metal Cations in Light Alkane Reactions Catalyzed by Modified H-ZSM5. *Catal. Today* **1996**, *31*, 207−231.

(11) Biscardi, J. A.; Iglesia, E. Reaction Pathways and Rate-Determining Steps in Reactions of Alkanes on H-ZSM5 and Zn/H-ZSM5 Catalysts. *J. Catal.* **1999**, *182*, 117−128.

(12) Biscardi, J. A.; Iglesia, E. Non-Oxidative Reactions of Propane on Zn/Na-ZSM5. *Phys. Chem. Chem. Phys.* **1999**, *1*, 5753−5759.

(13) Almutairi, S. M. T.; Mezari, B.; Magusin, P. C. M. M.; Pidko, E. A.; Hensen, E. J. M. Structure and Reactivity of Zn-Modified ZSM-5 Zeolites: The Importance of Clustered Cationic Zn Complexes. *ACS Catal.* **2012**, *2*, 71−83.

(14) Berndt, H.; Lietz, G.; Lücke, B.; Völter, J. Zinc Promoted H-ZSM-5 Catalysts for Conversion of Propane to Aromatics I. Acidity and Activity. *Appl. Catal., A* **1996**, *146*, 351−363.

(15) Berndt, H.; Lietz, G.; Völter, J. Zinc Promoted H-ZSM-5 Catalysts for Conversion of Propane to Aromatics II. Nature of the Active Sites and Their Activation. *Appl. Catal., A.* **1996**, *146*, 365−379.

(16) Kwak, B. S.; Sachtler, W. M. H. Aromatization of Propane over Zn/HZSM-5 Catalysts Prepared by Chemical Vapor Deposition. *Korean J. Chem. Eng.* **1996**, *13*, 356−363.

(17) Guisnet, M.; Gnep, N. S.; Vasques, H.; Ribeiro, F. R. Zn-Doped HZSM5 Catalysts for Propane Aromatization. In *Zeolite Chemistry and Catalysis*; Jacobs, P. A.; Jaeger, N. I.; Kubelková, L.; Wichterlová, B., Eds.; Elsevier: Amsterdam, 1991; pp 321−329.
(18) El-Malki, E.-M.; van Santen, R. A.; Sachtler, W. M. H. Introduction of Zn, Ga, and Fe into HZSM-5 Cavities by Sublimation: Identification of Acid Sites. *J. Phys. Chem. B* **1999**, *103*, 4611−4622.
(19) Kolyagin, Y. G.; Ivanova, I. I.; Pirogov, Y. A. ^{1}H and ^{13}C MAS NMR Studies of Light Alkanes Activation over MFI Zeolite Modified by Zn Vapour. *Solid State Nucl. Magn. Reson.* **2009**, *35*, 104−112.
(20) Kolyagin, Y. G.; Ivanova, I. I.; Ordomsky, V. V.; Gedeon, A.; Pirogov, Y. A. Methane Activation over Zn-Modified MFI Zeolite: NMR Evidence for Zn-Methyl Surface Species Formation. *J. Phys. Chem. C* **2008**, *112*, 20065−20069.
(21) Wang, X.; Xu, J.; Qi, G.; Wang, C.; Wang, W.; Gao, P.; Wang, Q.; Liu, X.; Feng, N.; Deng, F. Carbonylation of Ethane with Carbon Monoxide over Zn-Modified ZSM-5 Zeolites Studied by in Situ Solid-State NMR Spectroscopy. *J. Catal.* **2017**, *345*, 228−235.
(22) Xu, J.; Zheng, A.; Wang, X.; Qi, G.; Su, J.; Du, J.; Gan, Z.; Wu, J.; Wang, W.; Deng, F. Room Temperature Activation of Methane over Zn Modified H-ZSM-5 Zeolites: Insight from Solid-State NMR and Theoretical Calculations. *Chem. Sci.* **2012**, *3*, 2932.
(23) Wang, X.; Qi, G.; Xu, J.; Li, B.; Wang, C.; Deng, F. NMR-Spectroscopic Evidence of Intermediate-Dependent Pathways for Acetic Acid Formation from Methane and Carbon Monoxide over a ZnZSM-5 Zeolite Catalyst. *Angew. Chem., Int. Ed.* **2012**, *51*, 3850−3853.
(24) Kazansky, V. B.; Serykh, A. I. Unusual Localization of Zinc Cations in MFI Zeolites Modified by Different Ways of Preparation. *Phys. Chem. Chem. Phys.* **2004**, *6*, 3760−3764.
(25) Subbotina, I. R.; Kazansky, V. B. Two Alternative Mechanisms of Aromatization of Light Hydrocarbons on Ga/ZSM-5 and Zn/ZSM-5 Zeolites. *Pet. Chem.* **2009**, *49*, 11−15.
(26) Kazansky, V. B.; Serykh, A. A New Charge Alternating Model of Localization of Bivalent Cations in High Silica Zeolites with Distantly Placed Aluminum Atoms in the Framework. *Microporous Mesoporous Mater.* **2004**, *70*, 151−154.
(27) Kazansky, V. B.; Pidko, E. A. Intensities of IR Stretching Bands as a Criterion of Polarization and Initial Chemical Activation of Adsorbed Molecules in Acid Catalysis. Ethane Adsorption and Dehydrogenation by Zinc Ions in ZnZSM-5 Zeolite. *J. Phys. Chem. B* **2005**, *109*, 2103−2108.
(28) Kazansky, V. B.; Subbotina, I. R.; Rane, N.; van Santen, R. A.; Hensen, E. J. M. On Two Alternative Mechanisms of Ethane Activation over ZSM-5 Zeolite Modified by Zn^{2+} and Ga^{1+} Cations. *Phys. Chem. Chem. Phys.* **2005**, *7*, 3088−3092.
(29) Kazansky, V. B. Localization of Bivalent Transition Metal Ions in High-Silica Zeolites with the Very Broad Range of Si/Al Ratios in the Framework Probed by Low-Temperature H_2 Adsorption. *J. Catal.* **2003**, *216*, 192−202.
(30) Tamiyakul, S.; Sooknoi, T.; Lobban, L. L.; Jongpatiwut, S. Generation of Reductive Zn Species over Zn/HZSM−5 Catalysts for n−Pentane Aromatization. *Appl. Catal., A.* **2016**, *525*, 190−196.
(31) Du, Y.-J.; Hu, W.-D.; Wang, C.-M.; Zhou, J.; Yang, G.; Wang, Y.-D.; Yang, W.-M. First-Principles Microkinetic Analysis of Lewis Acid Sites in Zn-ZSM-5 for Alkane Dehydrogenation and Its Implication to Methanol-to-Aromatics Conversion. *Catal. Sci. Technol.* **2021**, *11*, 2031−2046.
(32) Oda, A.; Ohkubo, T.; Yumura, T.; Kobayashi, H.; Kuroda, Y. Why Do Zeolites Induce an Unprecedented Electronic State on Exchanged Metal Ions? *Phys. Chem. Chem. Phys.* **2017**, *19*, 25105−25114.
(33) Kazansky, V. B.; Serykh, A. I.; Anderson, B. G.; van Santen, R. A. The Sites of Molecular and Dissociative Hydrogen Adsorption in High-Silica Zeolites Modified with Zinc Ions. III DRIFT Study of H_2 Adsorption by the Zeolites with Different Zinc Content and Si/Al Ratios in the Framework. *Catal. Lett.* **2003**, *88*, 211−217.
(34) Oda, A.; Torigoe, H.; Itadani, A.; Ohkubo, T.; Yumura, T.; Kobayashi, H.; Kuroda, Y. Unprecedented Reversible Redox Process in the ZnMFI-H_2 System Involving Formation of Stable Atomic Zn^0. *Angew. Chem., Int. Ed.* **2012**, *51*, 7719−7723.
(35) Oda, A.; Torigoe, H.; Itadani, A.; Ohkubo, T.; Yumura, T.; Kobayashi, H.; Kuroda, Y. Mechanism of CH_4 Activation on a Monomeric Zn^{2+}-Ion Exchanged in MFI-Type Zeolite with a Specific Al Arrangement: Similarity to the Activation Site for H_2. *J. Phys. Chem. C* **2013**, 130917083323008.
(36) Karge, H. G. Solid-State Ion Exchange in Zeolites. In *Handbook of Heterogeneous Catalysis*; Wiley-VCH, 2008; Vol. *1*, pp 484−510.
(37) Dyer, A. Ion-Exchange Properties of Zeolites. In *Studies in Surface Science and Catalysis*; Čejka, J.; Van Bekkum, H., Eds.; Elsevier, 2005; Vol. *157*, pp 181−204.
(38) Ravel, B.; Newville, M. ATHENA, ARTEMIS, HEPHAESTUS: Data Analysis for X-Ray Absorption Spectroscopy Using IFEFFIT. *J. Synchrotron Radiat.* **2005**, *12*, 537−541.
(39) McCusker, L. B.; Baerlocher, C. Zeolite Structures. In *Studies in Surface Science and Catalysis*; van Bekkum, H.; Flanigan, E. M.; Jacobs, P. A.; Jansen, J. C., Eds.; Elsevier, 2001; Vol. *137*, pp 37−67.
(40) Heemsoth, J.; Tegeler, E.; Roessner, F.; Hagen, A. Generation of Active Sites for Ethane Aromatization in ZSM-5 Zeolites by a Solid-State Reaction of Zinc Metal with Brønsted Acid Sites of the Zeolite. *Microporous Mesoporous Mater.* **2001**, *46*, 185−190.
(41) Das, J.; Pradhan, S. K.; Sahu, D. R.; Mishra, D. K.; Sarangi, S. N.; Nayak, B. B.; Verma, S.; Roul, B. K. Micro-Raman and XPS Studies of Pure ZnO Ceramics. *Phys. B: Condens. Matter* **2010**, *405*, 2492−2497.
(42) Trivedi, M. K.; Sethi, K. K.; Panda, P.; Jana, S. A Comprehensive Physicochemical, Thermal, and Spectroscopic Characterization of Zinc (II) Chloride Using X-ray Diffraction, Particle Size Distribution, Differential Scanning Calorimetry, Thermogravimetric Analysis/Differential Thermogravimetric Analysis. *Int. J. Pharm. Invest.* **2017**, *7*, 33−40.
(43) Lercher, J. A.; Jentys, A. Infrared and Raman Spectroscopy for Characterizing Zeolites. In *Studies in Surface Science and Catalysis*; Čejka, J.; Van Bekkum, H.; Corma, A.; Schüth, F., Eds.; Elsevier, 2007; Vol. *168*, pp 435−476.
(44) Ong, L. H.; Dömök, M.; Olindo, R.; van Veen, A. C.; Lercher, J. A. Dealumination of HZSM-5 via Steam-Treatment. *Microporous Mesoporous Mater.* **2012**, *164*, 9−20.
(45) van Bokhoven, J. A.; van der Eerden, A. M. J.; Koningsberger, D. C. Three-Coordinate Aluminum in Zeolites Observed with In Situ X-Ray Absorption Near-Edge Spectroscopy at the Al K-Edge: Flexibility of Aluminum Coordinations in Zeolites. *J. Am. Chem. Soc.* **2003**, *125*, 7435−7442.
(46) Parry, E. P. An Infrared Study of Pyridine Adsorbed on Acidic Solids. Characterization of Surface Acidity. *J. Catal.* **1963**, *2*, 371−379.
(47) Liu, P.; Li, Z.; Liu, X.; Song, W.; Peng, B.; Zhang, X.; Nie, S.; Zeng, P.; Zhang, Z.; Gao, X.; Shen, B. Steaming Drived Chemical Interactions of $ZnCl_x$ with Y Zeolite Framework, Its Regulation to Dealumination/Silicon-Healing as Well as Enhanced Availability of Brønsted Acidity. *ACS Catal.* **2020**, *10*, 9197−9214.
(48) Hunger, M. Multinuclear Solid-State NMR Studies of Acidic and Non-Acidic Hydroxyl Protons in Zeolites. *Solid State Nucl. Magn. Reson.* **1996**, *6*, 1−29.
(49) Wang, M.; Jaegers, N. R.; Lee, M. S.; Wan, C.; Hu, J. Z.; Shi, H.; Mei, D.; Burton, S. D.; Camaioni, D. M.; Gutiérrez, O. Y.; Glezakou, V. A.; Rousseau, R.; Wang, Y.; Lercher, J. A. Genesis and Stability of Hydronium Ions in Zeolite Channels. *J. Am. Chem. Soc.* **2019**, *141*, 3444−3455.
(50) Stepanov, A. G. Basics of Solid-State NMR for Application in Zeolite Science: Material and Reaction Characterization. In *Zeolite and Zeolite-Like Materials*; Sels, B. F.; Kustov, L. M., Eds.; Elsevier, 2016; pp 137−188.
(51) Gackowski, M.; Podobinski, J.; Broclawik, E.; Datka, J. IR and NMR Studies of the Status of Al and Acid Sites in Desilicated Zeolite Y. *Molecules* **2020**, *25*, 31.

https://doi.org/10.1021/acscatal.1c03641
ACS Catal. 2021, 11, 14489−14506

(52) van Bokhoven, J. A.; Roest, A. L.; Koningsberger, D. C.; Miller, J. T.; Nachtegaal, G. H.; Kentgens, A. P. M. Changes in Structural and Electronic Properties of the Zeolite Framework Induced by Extraframework Al and La in H-USY and La(x)NaY: A ^{29}Si and ^{27}Al MAS NMR and ^{27}Al MQ MAS NMR Study. *J. Phys. Chem. B* **2000**, *104*, 6743−6754.
(53) Yang, C.; Zhu, W.; Sen, S.; Castro, R. H. R. Site Inversion Induces Thermodynamic Stability against Coarsening in Zinc Aluminate Spinel. *J. Phys. Chem. C* **2019**, *123*, 8818−8826.
(54) Fabián, M.; Bottke, P.; Girman, V.; Düvel, A.; Da Silva, K. L.; Wilkening, M.; Hahn, H.; Heitjans, P.; Šepelák, V. A Simple and Straightforward Mechanochemical Synthesis of the Far-from-Equilibrium Zinc Aluminate, $ZnAl_2O_4$, and Its Response to Thermal Treatment. *RSC Adv.* **2015**, *5*, 54321−54328.
(55) Sameera, S.; Vidyadharan, V.; Sasidharan, S.; Gopchandran, K. G. Nanostructured Zinc Aluminates: A Promising Material for Cool Roof Coating. *J. Sci. Adv. Mater. Devices* **2019**, *4*, 524−530.
(56) Chen, C.; Hu, Z.; Ren, J.; Zhang, S.; Wang, Z.; Yuan, Z.-Y. ZnO Nanoclusters Supported on Dealuminated Zeolite β as a Novel Catalyst for Direct Dehydrogenation of Propane to Propylene. *ChemCatChem* **2019**, *11*, 868−877.
(57) Chen, J.; Feng, Z.; Ying, P.; Li, C. ZnO Clusters Encapsulated Inside Micropores of Zeolites Studied by UV Raman and Laser-Induced Luminescence Spectroscopies. *J. Phys. Chem. B* **2004**, *108*, 12669−12676.
(58) Castorina, E.; Ingall, E. D.; Morton, P. L.; Tavakoli, D. A.; Lai, B. Zinc K-Edge XANES Spectroscopy of Mineral and Organic Standards. *J. Synchrotron Radiat.* **2019**, *26*, 1302−1309.
(59) Pinilla-Herrero, I.; Borfecchia, E.; Holzinger, J.; Mentzel, U. V.; Joensen, F.; Lomachenko, K. A.; Bordiga, S.; Lamberti, C.; Berlier, G.; Olsbye, U.; Svelle, S.; Skibsted, J.; Beato, P. High Zn/Al Ratios Enhance Dehydrogenation vs Hydrogen Transfer Reactions of Zn-ZSM-5 Catalytic Systems in Methanol Conversion to Aromatics. *J. Catal.* **2018**, *362*, 146−163.
(60) Mosallanejad, S.; Dlugogorski, B. Z.; Kennedy, E. M.; Stockenhuber, M. HCl Adsorption on Copper-Modified ZSM-5: FTIR and DFT Study. *J. Phys. Chem. C* **2013**, 130912084723007.
(61) Schmidt, S. A.; Kumar, N.; Shchukarev, A.; Eränen, K.; Mikkola, J.-P.; Murzin, D. Y.; Salmi, T. Preparation and Characterization of Neat and $ZnCl_2$ Modified Zeolites and Alumina for Methyl Chloride Synthesis. *Appl. Catal., A.* **2013**, *468*, 120−134.
(62) Kytökivi, A.; Lindblad, M.; Root, A. IR and ^{1}H NMR Studies on the Adsorption of Gaseous Hydrogen Chloride on γ-Alumina. *J. Chem. Soc. Faraday Trans.* **1995**, *91*, 941−948.
(63) Schweitzer, N. M.; Hu, B.; Das, U.; Kim, H.; Greeley, J.; Curtiss, L. A.; Stair, P. C.; Miller, J. T.; Hock, A. S. Propylene Hydrogenation and Propane Dehydrogenation by a Single-Site Zn^{2+} on Silica Catalyst. *ACS Catal.* **2014**, *4*, 1091−1098.
(64) Camacho-Bunquin, J.; Aich, P.; Ferrandon, M.; Getsoian, A. "Bean".; Das, U.; Dogan, F.; Curtiss, L. A.; Miller, J. T.; Marshall, C. L.; Hock, A. S.; Stair, P. C. Single-Site Zinc on Silica Catalysts for Propylene Hydrogenation and Propane Dehydrogenation: Synthesis and Reactivity Evaluation Using an Integrated Atomic Layer Deposition-Catalysis Instrument. *J. Catal.* **2017**, *345*, 170−182.
(65) Mahyuddin, M. H.; Tanaka, S.; Shiota, Y.; Yoshizawa, K. Room-Temperature Activation of Methane and Direct Formations of Acetic Acid and Methanol on Zn-ZSM-5 Zeolite: A Mechanistic DFT Study. *Bull. Chem. Soc. Jpn.* **2020**, *93*, 345−354.
(66) Frash, M. V.; Van Santen, R. A. Activation of Ethane in Zn-Exchanged Zeolites: A Theoretical Study. *Phys. Chem. Chem. Phys.* **2000**, *2*, 1085−1089.
(67) Pidko, E. A.; van Santen, R. A. Activation of Light Alkanes over Zinc Species Stabilized in ZSM-5 Zeolite: A Comprehensive DFT Study. *J. Phys. Chem. C.* **2007**, *111*, 2643−2655.
(68) Barbosa, L. A. M. M.; van Santen, R. A. The Activation of H_2 by Zeolitic Zn(II) Cations. *J. Phys. Chem. C.* **2007**, *111*, 8337−8348.
(69) Janda, A.; Bell, A. T. Effects of Si/Al Ratio on the Distribution of Framework Al and on the Rates of Alkane Monomolecular Cracking and Dehydrogenation in H-MFI. *J. Am. Chem. Soc.* **2013**, *135*, 19193−19207.
(70) Narbeshuber, T. F.; Vinek, H.; Lercher, J. A. Monomolecular Conversion of Light Alkanes over H-ZSM-5. *J. Catal.* **1995**, *157*, 388−395.
(71) Narbeshuber, T. F.; Brait, A.; Seshan, K.; Lercher, J. A. Dehydrogenation of Light Alkanes over Zeolites. *J. Catal.* **1997**, *172*, 127−136.
(72) Xu, B.; Sievers, C.; Hong, S. B.; Prins, R.; van Bokhoven, J. A. Catalytic Activity of Brønsted Acid Sites in Zeolites: Intrinsic Activity, Rate-Limiting Step, and Influence of the Local Structure of the Acid Sites. *J. Catal.* **2006**, *244*, 163−168.
(73) Gounder, R.; Iglesia, E. Catalytic Consequences of Spatial Constraints and Acid Site Location for Monomolecular Alkane Activation on Zeolites. *J. Am. Chem. Soc.* **2009**, *131*, 1958−1971.
(74) Arzumanov, S. S.; Gabrienko, A. A.; Toktarev, A. V.; Freude, D.; Haase, J.; Stepanov, A. G. Propane Activation on Zn-Modified Zeolite. The Effect of the Nature of Zn-Species on the Mechanism of H/D Hydrogen Exchange of the Alkane with Brønsted Acid Sites. *J. Catal.* **2019**, *378*, 341−352.
(75) Arzumanov, S. S.; Gabrienko, A. A.; Toktarev, A. V.; Lashchinskaya, Z. N.; Freude, D.; Haase, J.; Stepanov, A. G. Propane Transformation on Zn-Modified Zeolite. Effect of the Nature of Zn Species on Alkane Aromatization and Hydrogenolysis. *J. Phys. Chem. C* **2019**, *123*, 30473−30485.
(76) Arzumanov, S. S.; Gabrienko, A. A.; Toktarev, A. V.; Freude, D.; Haase, J.; Stepanov, A. G. Mechanism of H/D Hydrogen Exchange of n-Butane with Brønsted Acid Sites on Zn-Modified Zeolite: The Effect of Different Zn Species (Zn^{2+} and ZnO) on the Activation of Alkane C-H Bonds. *J. Phys. Chem. C* **2020**, *124*, 20270−20279.
(77) Pinilla-Herrero, I.; Borfecchia, E.; Cordero-Lanzac, T.; Mentzel, U. V.; Joensen, F.; Lomachenko, K. A.; Bordiga, S.; Olsbye, U.; Beato, P.; Svelle, S. Finding the Active Species: The Conversion of Methanol to Aromatics over Zn-ZSM-5/Alumina Shaped Catalysts. *J. Catal.* **2021**, *394*, 416−428.
(78) Dědeček, J.; Sobalík, Z.; Wichterlová, B. Siting and Distribution of Framework Aluminium Atoms in Silicon-Rich Zeolites and Impact on Catalysis. *Catal. Rev.* **2012**, *54*, 135−223.
(79) van Santen, R. A.; Zhidomirov, G. M.; Shubin, A. A.; Yakovlev, A. L.; Barbosa, L. A. M. M. Reactivity Theory of Zinc Cation Species in Zeolites. In *Catalysis by Unique Metal Ion Structures in Solid Matrices*; Centi, G.; Wichterlová, B.; Bell, A. T., Eds.; Kluwer Academic Publishers, 2001; pp 187−204.
(80) Benco, L.; Bucko, T.; Hafner, J.; Toulhoat, H. Periodic DFT Calculations of the Stability of Al/Si Substitutions and Extraframework Zn^{2+} Cations in Mordenite and Reaction Pathway for the Dissociation of H_2 and CH_4. *J. Phys. Chem. B* **2005**, *109*, 20361−20369.
(81) Albarracín-Suazo, S. C.; Pagán-Torres, Y. J.; Curet-Arana, M. C. DFT Study on the Effect of Aluminum Position in Zn-Exchanged MFI on Methane Activation. *J. Phys. Chem. C* **2019**, *123*, 16164−16171.
(82) Song, C.; Chu, Y.; Wang, M.; Shi, H.; Zhao, L.; Guo, X.; Yang, W.; Shen, J.; Xue, N.; Peng, L.; Ding, W. Cooperativity of Adjacent Brønsted Acid Sites in MFI Zeolite Channel Leads to Enhanced Polarization and Cracking of Alkanes. *J. Catal.* **2017**, *349*, 163−174.
(83) Bernauer, M.; Tabor, E.; Pashkova, V.; Kaucký, D.; Sobalík, Z.; Wichterlová, B.; Dedecek, J. Proton Proximity − New Key Parameter Controlling Adsorption, Desorption and Activity in Propene Oligomerization over H-ZSM-5 Zeolites. *J. Catal.* **2016**, *344*, 157−172.
(84) Roshanaei, A.; Alavi, S. M. Kinetic Study of Propane Aromatization over Zn/HZSM-5 Zeolite under Conditions of Catalyst Deactivation Using Genetic Algorithm. *J. Serb. Chem. Soc.* **2018**, *83*, 473−488.

https://doi.org/10.1021/acscatal.1c03641
ACS Catal. 2021, 11, 14489−14506